



RESEARCH ARTICLE

10.1029/2021JG006359

Key Points:

- A carbon budget shows that microbial metabolism is the dominant organic carbon transformation pathway in a typical Norwegian boreal lake
- At least 35% of the organic carbon exported from a typical South Norwegian catchment is mineralized before reaching the fjord
- Over 67% of the organic carbon mineralization occurs in the headwater catchment highlighting the role of headwaters in carbon cycling

Supporting Information:

Supporting Information may be found in the online version of this article.

Correspondence to:

F. Clayer,
francois.clayer@niva.no

Citation:

Clayer, F., Thrane, J.-E., Brandt, U., Dörsch, P., & de Wit, H. A. (2021). Boreal headwater catchment as hot spot of carbon processing from headwater to fjord. *Journal of Geophysical Research: Biogeosciences*, 126, e2021JG006359. <https://doi.org/10.1029/2021JG006359>

Received 25 MAR 2021

Accepted 25 OCT 2021

Author Contributions:

Conceptualization: F. Clayer, J.-E.

Thrane, H. A. Wit

Formal analysis: J.-E. Thrane, P. Dörsch

Funding acquisition: H. A. Wit

Methodology: F. Clayer, J.-E. Thrane, U. Brandt, P. Dörsch

Project Administration: F. Clayer

Resources: F. Clayer, U. Brandt, P.

Dörsch, H. A. Wit


Software: U. Brandt

Validation: F. Clayer, H. A. Wit

Visualization: F. Clayer

Writing – original draft: F. Clayer

Boreal Headwater Catchment as Hot Spot of Carbon Processing From Headwater to Fjord

F. Clayer¹ , J.-E. Thrane¹, U. Brandt¹, P. Dörsch² , and H. A. de Wit^{1,3} 

¹Norwegian Institute for Water Research (NIVA), Oslo, Norway, ²Norwegian University of Life Sciences (NMBU), Ås, Norway, ³Centre for Biogeochemistry in the Anthropocene, University in Oslo, Oslo, Norway

Abstract Boreal headwaters and aquatic sediments are significant transporters, stores and processors of terrestrial carbon (C) as well as emitters of greenhouse gases (GHGs), mainly CO₂ and CH₄. While terrestrial ecosystems are net sinks of atmospheric C, lateral fluxes of total organic and dissolved inorganic C (TOC, DIC) as well as GHG release can significantly reduce the land C sink. However, the fate of the laterally exported C remains often unresolved. Here, we combine datasets from high-frequency sensors, monitoring and modeling to produce a C budget for a typical boreal lake and its catchment and examine it in a regional context. We show that lake TOC removal is dominated by microbial metabolism which shows strong seasonal fluctuations following stratification and ice-cover dynamics. We estimate that 11.5 g C m⁻² catchment yr⁻¹ are exported from the catchment soils and wetlands, including 9.5 g of TOC. Only 5.4 g C m⁻² catchment yr⁻¹ reach the coast while over 50% is reemitted to the atmosphere (5.7 g C m⁻² catchment yr⁻¹). Part of the reemitted C originates from rapid turnover cycles and would not affect atmospheric CO₂ and the land C sink. However, we show that the land C sink at Langtjern is reduced by >14% over the whole aquatic continuum, and by >10% within the headwater catchment. Our regional analysis suggests that headwater lake TOC mineralization is the main TOC loss along the aquatic continuum with burial being relatively small, and highlights the significance of small headwaters as intensive and fast-responding TOC processors.

Plain Language Summary Small boreal lakes and streams are intensive sites of carbon (C) processing and greenhouse gas (GHG) emissions. While trees and other plants in the boreal forest capture atmospheric C, soil C losses through aquatic export of organic C and GHG evasion can reduce this land C capture with consequences on global warming and the climate system. The magnitude of these aquatic fluxes remain largely unresolved. In this study, we quantified the C fluxes from Norwegian mountainous (moderate elevation) lakes and streams to fjord and show that mountainous aquatic environments are fast-responding and intensive sites of C processing. More than 35% of the organic C exported from soils is transformed to GHG before reaching the fjord, of which 67% happens within 4 km of C fixation in the forest. In total, we estimate that about 20% of the C fixed in the forest, likely more, is counterbalanced by GHG emissions from aquatic environments, especially within small lakes and streams.

1. Introduction

Freshwaters are key interfaces connecting the various Earth compartments. Soil and wetland organic carbon (C), originating from photosynthetic activity in the biosphere (Arndt et al., 2013), is leached to surface waters where it is processed in the water column and in aquatic sediments before being either reemitted to the atmosphere or buried in the geosphere (Tissot & Welte, 1984). Thus, the hydrosphere plays an important role in global element cycles transferring significant amounts of energy, C and other elements from the biosphere to the geosphere and the atmosphere. Yet, the hydrosphere is probably the most poorly represented component in Earth System Models (ESM; e.g., CLM5; Lawrence et al., 2018). Including aquatic C transport and evasion in the assessment of the land C sink, that is, net ecosystem productivity (NEP; Randerson et al., 2002), is conceptually straightforward and involves incorporation of all C fluxes in an ecosystem including lateral C fluxes of autotrophic and heterotrophic origin. While the land C sink in ESMs is simulated as the balance between photosynthesis and respiration (Randerson et al., 2009), lateral freshwater C fluxes are usually ignored (e.g., CLM5; Lawrence et al., 2018). Lateral fluxes of TOC and DIC as well as greenhouse gases (GHGs) release can reduce the land C sink by up to a third in peatland catchments and by 20% in productive forested catchments (Butman et al., 2016; Chi et al., 2020; de Wit, Ledesma, & Futter, 2016; Öquist et al., 2014; Wallin et al., 2018; Webb et al., 2019).

© 2021 The Authors.

This is an open access article under the terms of the [Creative Commons Attribution-NonCommercial License](https://creativecommons.org/licenses/by-nc/4.0/), which permits use, distribution and reproduction in any medium, provided the original work is properly cited and is not used for commercial purposes.

Writing – review & editing: F. Clayer, J.-E. Thrane, P. Dörsch, H. A. Wit

Headwater catchments represent one end-member of the Earth continental system where all key interfaces (i.e., atmosphere-biosphere, geosphere-hydrosphere-atmosphere) converge creating steep biological, chemical and physical gradients. Hence, small catchments (<10 km²) are sites of intensive terrestrial C recycling (Holgerson & Raymond, 2016; Staehr et al., 2012). The pivotal role of aquatic pathways in the global C budget has been acknowledged for over a decade (Ciais et al., 2013; Cole et al., 2007). Especially in the lake-rich (Verpoorter et al., 2014) and wet C-rich boreal forest region which holds ~50% of the world's forest C stock (Deluca & Boisvenue, 2012), lakes are hotspots of CO₂ and CH₄ release (Hastie et al., 2018; Wallin et al., 2018; Wik et al., 2016).

The magnitude of the land C sink is critically linked to the fate of the C transported laterally along the aquatic continuum from mountain to sea and its mineralization during transport (Butman et al., 2016). Southern Norway is an example for a carbon-rich landscape with large proportion of lakes and rivers, and steep topographic gradients with implications on the water residence time. Along this continuum, various mechanisms show potential contrasting impacts on the role of water courses in the C cycle. On the one hand, coastal mountainous regions with flashy rivers are effective transporters of C from land to sea (Hilton et al., 2011). Furthermore, fjords are sites of intensive organic C burial and are argued to play an important role in climate regulation (Smith et al., 2015). On the other hand, organic C decay rates in aquatic systems have been shown to be inversely related to the water retention time (Catalán et al., 2016). Additionally, mountainous streams emit large quantities of CO₂ as a result of turbulent flows (Horgby et al., 2019). Hence, the functioning of the aquatic continuum as a 'reactor' in carbon-rich, wet landscapes with steep topographic gradients such as found in Southern Norway needs to be further elucidated (de Wit et al., 2018).

In a previous study, a 30-year record (1986–2015) of inlet and outlet TOC in the highly instrumented boreal lake site Langtjern was combined with process-based modeling of lake DOC processing to draw a lake C budget (de Wit et al., 2018). Lake removal of TOC—on average 8% of TOC inputs—was primarily attributed to microbial metabolism, with burial as the second-most important removal process. Since 2015, continuous high-frequency monitoring of outlet CO₂ concentrations and inlet discharge was initiated. In addition, periodic field measurements of GHG concentrations in lake, inlet and outlet streams, as well as lake CO₂ effluxes were carried out. Here, in light of this new dataset, we produce a new lake C budget for the period 2015 to 2019, including organic and inorganic C fluxes. The inorganic carbon fluxes estimated from floating CO₂ flux chambers, high-frequency pCO₂ sensor and targeted sampling allowed to better appreciate the importance of the lake as processor of organic C. We further show that lake organic C processing was previously underestimated. Process-based modeling of lake DOC is used to partition lake organic C removal among various processes. We use this case study, embedded in a regional carbon budget from headwater to fjord, to investigate the role of boreal headwaters as processors of organic C, representative for a carbon-rich boreal landscape with steep hydrological gradients.

2. Materials and Methods

2.1. Study Site

Langtjern, a small (4.8 km²; 510–750 m.a.s.l.; 60.371 N, 9.727 E) boreal catchment in southeast Norway (Figure 1), has been a research station under national monitoring programs for air pollution effects on hydrology and chemistry of surface waters starting in 1972 (de Wit et al., 2014, 2018) while investigations of climate effects started in 2010 (de Wit et al., 2018) through high-frequency monitoring of climate-sensitive parameters in inlet, lake and outlet. The catchment has relatively shallow soils and is 75% forested with low productivity Scots pine forest and 5% of productive Norway spruce forest, with the remaining 20% being peatlands. The forest is mature and has been mostly preserved from forest harvesting except for some small-scale forest harvest in the 1950s. Langtjern geological substrate consists of till generated from felsic gneisses and granites. Mean annual temperature, precipitation, and discharge (2015–2019) are 4.1°C, 921 mm, and 607 mm, respectively.

Lake—Lake Langtjern (0.23 km²) has a mean depth of 2 m, maximum of 12 m, and 9 m in the northern basin (where a buoy is located; Figure 1). It is fed by two main inlets (south and east) draining 60% of the catchment. The East inlet, equipped with a high-frequency monitoring station (see below), drains a sub-catchment of 0.8 km². The lake has a mean residence time of 2.2 ± 0.4 months, is dimictic and experiences thermal stratification in summer with a thermocline at 1–3 m depth. Mean pH, total organic carbon (TOC), total P, and total N

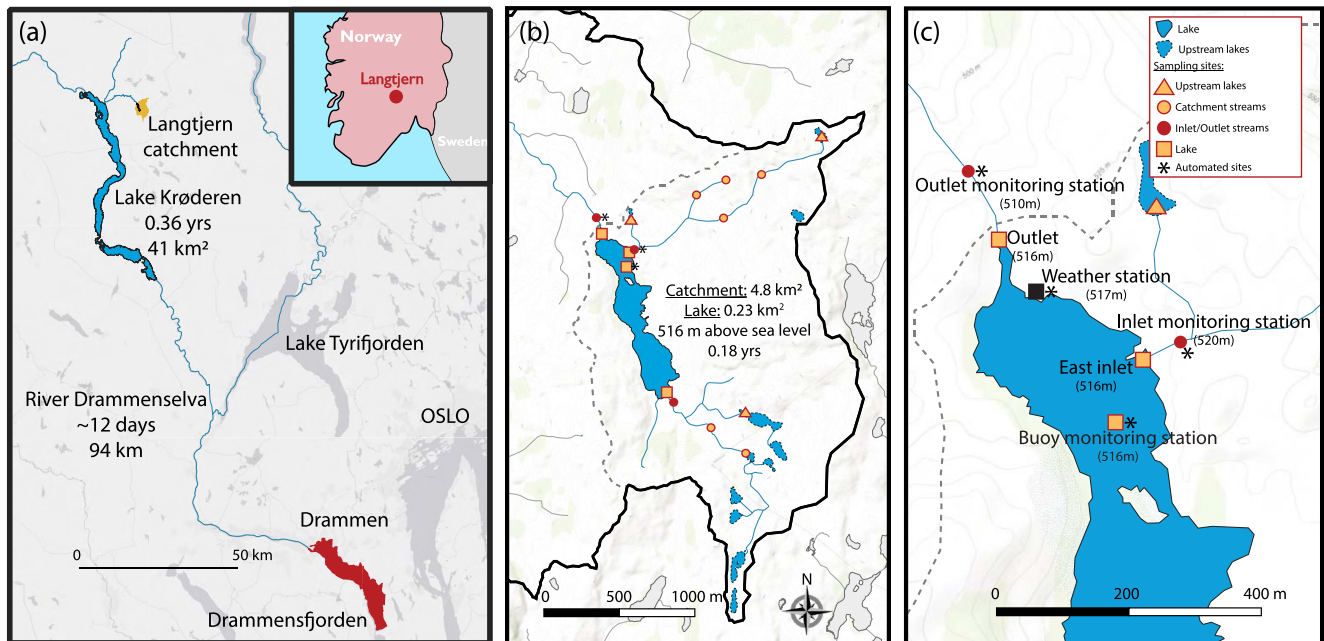


Figure 1. Map of Langtjern. Panel (a), water course from headwater Langtjern (yellow) to Drammen fjord (red). Numbers refer to water residence time, lake surface and length of water course. Panels (b) and (c), map and close-up of the Langtjern catchment showing sites for automated and manual sampling. In panel (c), elevation for each sampling site is given in parentheses.

(2015–2019) are 4.9 ± 0.3 , 11.8 ± 2.0 mg C L⁻¹, 5.2 ± 1.9 μg P L⁻¹, and 250 ± 46 μg N L⁻¹, respectively. Mean chlorophyll-a is <2 μg L⁻¹.

Headwater to coast continuum—Langtjern is part of the Skagerrak drainage basin comprising low-productive mountain ecosystems and more productive lowland forests with an average C uptake in biomass and soils (the sum of which is an estimate of NEP) of 28.4 g C m⁻² yr⁻¹ (de Wit et al., 2015). Water from Langtjern drains into Lake Krøderen (41 km²; 133 m.a.s.l.; mean and max. depth are 32 and 130 m; 60.327 N, 9.645 E) which has an average water retention time of 0.36 years (NVE Lake database 2020), and reaches the Drammensfjord through the river Drammenselva (Figure 1). Drammenselva has an average discharge of 325 m³ s⁻¹ and drains a 17,034-km² large catchment which is >90% natural with significant portions of forested (50%) and mountainous (20%) areas (Veitenberg Braaten et al., 2020). The section of Drammenselva from Lake Krøderen to the fjord is 94 km long along which another large tributary flowing out of Lake Tyrifjorden is joining the river (Figure 1a; NVE River network 2020). Assuming an average water velocity of 3 km hr⁻¹ (Feng et al., 2018), it has an average travel time of about 12 days. The 20-km long and 1.6–3.0-km wide Drammensfjord (maximum depth: 117 m) is isolated from the greater Oslofjord by a shallow sill at its Southern extremity (Smittenberg et al., 2005). Drammensfjord sediments accumulate organic C at an average rate of 25.3 g m⁻² yr⁻¹ (Huguet et al., 2007; Smith et al., 2015).

2.2. Monitoring and High-Frequency Data Sets

Discharge at the lake outlet (since autumn 2010) and the inlet monitoring station (since autumn 2014) were obtained by measuring bi-hourly water level at V notch weirs. Previously, inlet discharge was derived from the estimated partitioning of evapotranspiration between the catchment and the lake within a full water balance (described in de Wit et al., 2014). Now the inlet discharge is directly calculated from high-frequency measurements of water level at the V notch weir. This change in method yielded higher inlet discharge, attributing more of the evapotranspiration to the lake rather than the catchment (see Table S5 in Supporting Information S1).

Since 1986, water grab samples for TOC, total P and N were collected weekly and weekly to monthly at the outlet and inlet monitoring stations, respectively. Briefly, water was sampled according to procedures established in the acid monitoring program (SFT., 2009), sent to the Norwegian Institute for Water Research (NIVA) by mail and analyzed at the NIVA accredited laboratory following standard methods: (1) the NS-EN 1484:1997 method for

TOC with a Fusion TOC analyzer (Teledyne Tekmar), and (2) the NS 4725:1984 and NS 4743:1993 method for TOT-P and TOT-N, respectively, both with a Continuous Flow Analyzer (Skalar). Note that DOC is on average 94% of TOC at Langtjern (de Wit et al., 2018).

High frequency monitoring stations (Figure 1) have been deployed at the lake buoy (since 2013), the Eastern inlet (since summer 2014) and outlet (since 2010) recording sub-hourly to bi-hourly lake temperature (0.5, 1, 1.5, 2, 3, 4, 6, and 8 m depth), lake oxygen concentration (Oxygen Optode 3835, Aanderaa Instruments; 1 and 6 m depth), water temperature and fDOM (MicroFlu-CDOM, TriOS), as well as pH (Durafer II pH electrode with DL421 DirectLine sensor, Honeywell) and conductivity (graphite electrode DL400 with DL423 DirectLine sensor, Honeywell) at the outlet. Since October 2017, a pCO₂ sensor (Franatech AS; ±1% precision) was deployed at 0.5 m depth at the outlet monitoring station taking bihourly measurements. All sensor data are automatically saved onto a datalogger (CR1000, Campbell Scientific) and sent daily to NIVA databases for quality control and storage, and are presented on www.aquamonitor.no/langtjern (real-time, not quality assured). An on-site camera and a weather station, operating since 2010, provide daily photographs of the lake (taken at 12:00), as well as sub-hourly to hourly air temperature (CS215, Campbell Scientific), radiation (SP-212, Apogee), wind (mean, max, and direction; Wind Monitor Model 05,103, R. M. Young), relative humidity (CS215, Campbell Scientific) and precipitation (T-200B precipitation gauge, Geonor).

The lake mixing periods were defined as when the surface-to-bottom temperature difference was less than 1°C (Robertson & Ragotzkie, 1990). Ice-on and ice-off dates were determined based on daily lake webcam pictures and discontinuous ice-cover period was constrained from first sight of free lake surface on pictures to complete ice-off.

The dissolved CO₂ concentration ([CO₂]) was calculated from pCO₂ sensor data using Henry law:

$$[\text{CO}_2] = K_H [\text{CO}_2]_{\text{air}} P_{\text{atm}} \quad (1)$$

where K_H is the Henry constant for CO₂ adjusted for in-situ temperature (Stumm & Morgan, 1996), $[\text{CO}_2]_{\text{air}}$ is the pCO₂ and P_{atm} is the measured atmospheric pressure.

2.3. Lake DOC Modeling

A one-dimensional coupled physical-biogeochemical water-column model was used to model lake DOC and provide estimations of in-lake DOC process rates. The physical component, that is, General Ocean Turbulence Model Framework (GOTM (Bruggeman & Bolding, 2014), includes the main hydrodynamic and thermodynamic processes related to vertical mixing in natural waters, heat distribution across the water-column and through the water-air interface as well as ice-cover. The biogeochemical components included the Selma (<https://github.com/fabm-model/fabm/tree/master/src/models/selma>) and DOMCAST (<https://github.com/fabm-model/fabm/tree/master/src/models/niva/domcast>) modules deployed within the Framework for Aquatic Biogeochemical Models (FABM; Bruggeman & Bolding, 2014). Selma is an adaptation of the ERGOM model (Neumann et al., 2002) by the PROGNOS project (WATER JPI project: WaterWorks2014- PROGNOS) with upgrades related to oxygen dynamics between sediment and water as described by (Neumann & Schernewski, 2008). DOMCAST is a module representing the DOC processing as is also done in MyLake (de Wit et al., 2018) suitable for integrating high-frequency sensor data with water quality models in FABM. The three key processes implemented in DOMCAST for DOC processing have been already described earlier by de Wit et al. (2018). Briefly, the model considers: microbial metabolism through oxidic respiration and denitrification, photo-mineralization, and flocculation driven sedimentation. Metabolism and photo-mineralization both yield DIC, while flocculation yields POC. The sum of these three processes represent total lake carbon removal. The modeled processing rates for each of the three key processes provided by the calibrated model application are used below to constrain the lake C budget. The main distinction between MyLake and GOTM-Selma-DOMCAST is related to the oxygen sediment consumption. While MyLake is coupled to a sediment diagenesis module to account for sediment oxygen consumption (Couture et al., 2015), GOTM-Selma-DOMCAST relies on a sediment-oxygen demand approach (e.g., Rucinski et al., 2014) where the sediment oxygen consumption rate is a function of the sediment mineralization rate and the amount of settling detritus, supplied by DOC flocculation (DOMCAST) and stream inflows (Figure S1 in Supporting Information S1).

The coupled physical-biogeochemical model was calibrated using the ParSAC autocalibration tool (<https://bolding-bruggeman.com/portfolio/parsac/>) using the Maximum Likelihood optimization method based on the Nelder-Mead simplex algorithm (Nelder & Mead, 1965). The physical module was first calibrated against observed lake temperature, before calibrating the biogeochemical modules against observed outlet DOC as well as epi- and hypo-limnion O₂ concentrations. Calibration and validation periods were 2015–2017 and 2018–2019, respectively. The parameters considered during calibration were the scaling factors for short-wave solar radiation, surface heat fluxes, and wind, the minimum turbulent kinetic energy (TKE), the light extinction coefficient, the ice albedo, as well as the piston velocity for O₂ air-water exchange, mineralization rates in the sediment and its temperature control, the flocculation constant, the OM degradation constant and its temperature control (Table S1 in Supporting Information S1).

2.4. Sampling and Field Measures of Dissolved Gases

Surface water samples for dissolved gases (CO₂, CH₄, N₂O, and O₂) were gathered at 14 occasions over a 2-year period (2018–2019) at various times of year when the lake was ice-covered, mixed, or stratified (Figure 2). Samples were collected from a total of 16 sites in the catchment including lake pelagic, littoral and up-stream and down-stream stream sites (Figure 1). Profiles of water samples were also taken at 10 occasions at the deepest point of the Northern lake basin (9-m depth) with a vertical resolution of 2 m.

Water for dissolved gases analyses was collected in 120-mL glass bottle, filled and closed underwater with a gas-tight butyl-rubber septum with no headspace while minimizing turbulence to avoid gas loss. To preserve the sample, a small volume (0.4–0.6 mL) of a HgCl₂ solution (7 g L⁻¹) was added with a syringe through the closed septum while allowing an equivalent volume (0.4–0.6 mL) of water to escape from the bottle through a second needle. Samples were kept at 4°C until further processing in the laboratory.

Diffusive CO₂ flux measurements at the water-air interface included single measures at eight occasions over the 2-year period at up to 16 sites as well as two 24 hr campaigns with 3 to 4-hourly measurements. Fluxes were measured with self-made flux chambers as described by Bastviken et al. (2015). Briefly they consist of a plastic bucket equipped with a Senseair K30 sensor recording pCO₂, temperature and relative humidity every 30 s for a duration of 15–30 min. Three flux chambers were deployed at each site. The 24 hr flux campaigns were performed in May 2018 at the buoy and in July 2019 at the lake outlet, respectively (Figure 2). In July 2019, additional measurements were carried out twice a day (morning and evening) at the same site up to 48 hr after the 24 hr campaign. After retrieving sensor data, fluxes were calculated from the linear increase in pCO₂ corrected for ambient temperature and humidity in the chamber (Bastviken et al., 2015). Linear slopes showing a R² lower than 0.9 were automatically rejected. Collection of dissolved gas samples and flux measurements were performed at the same sites to allow calculation of the CO₂ gas exchange coefficient (k_{CO_2}) according to:

$$k_{\text{CO}_2} = \frac{F_{\text{CO}_2}}{[\text{CO}_2] - [\text{CO}_2]_{\text{eq}}} \quad (2)$$

where F_{CO_2} is the CO₂ flux in $\mu\text{mol m}^{-2} \text{h}^{-1}$ and $[\text{CO}_2]_{\text{eq}}$ is the theoretical water CO₂ concentration in equilibrium with atmospheric CO₂ concentration (407–410 ppm, NOAA) calculated with Equation 1. The gas exchange coefficient was then standardized to a Schmidt number of 600 using

$$k_{600} = k_{\text{CO}_2} \left(\frac{600}{S_{\text{CO}_2}} \right)^n \quad (3)$$

where S_{CO_2} is the CO₂ Schmidt number for a given temperature (Wanninkhof, 2014). We used $n = 2/3$ since 99% of the time wind speed was below 3.7 m s⁻¹ (Guérin et al., 2007).

2.5. Dissolved Gas Analyses

Dissolved gas samples were analyzed for CO₂, CH₄, N₂O and O₂ by headspace technique as described in detail by Yang et al. (2015). Briefly, after room temperature equilibration, bottles were backfilled with 20–30 mL Helium (He) at atmospheric pressure and shaken for 2 hr for gas equilibration. Following shaking, 2 mL of headspace gas were sampled (autosampler GC-Pal, CTC, Switzerland) and injected into a gas chromatograph (GC) with He

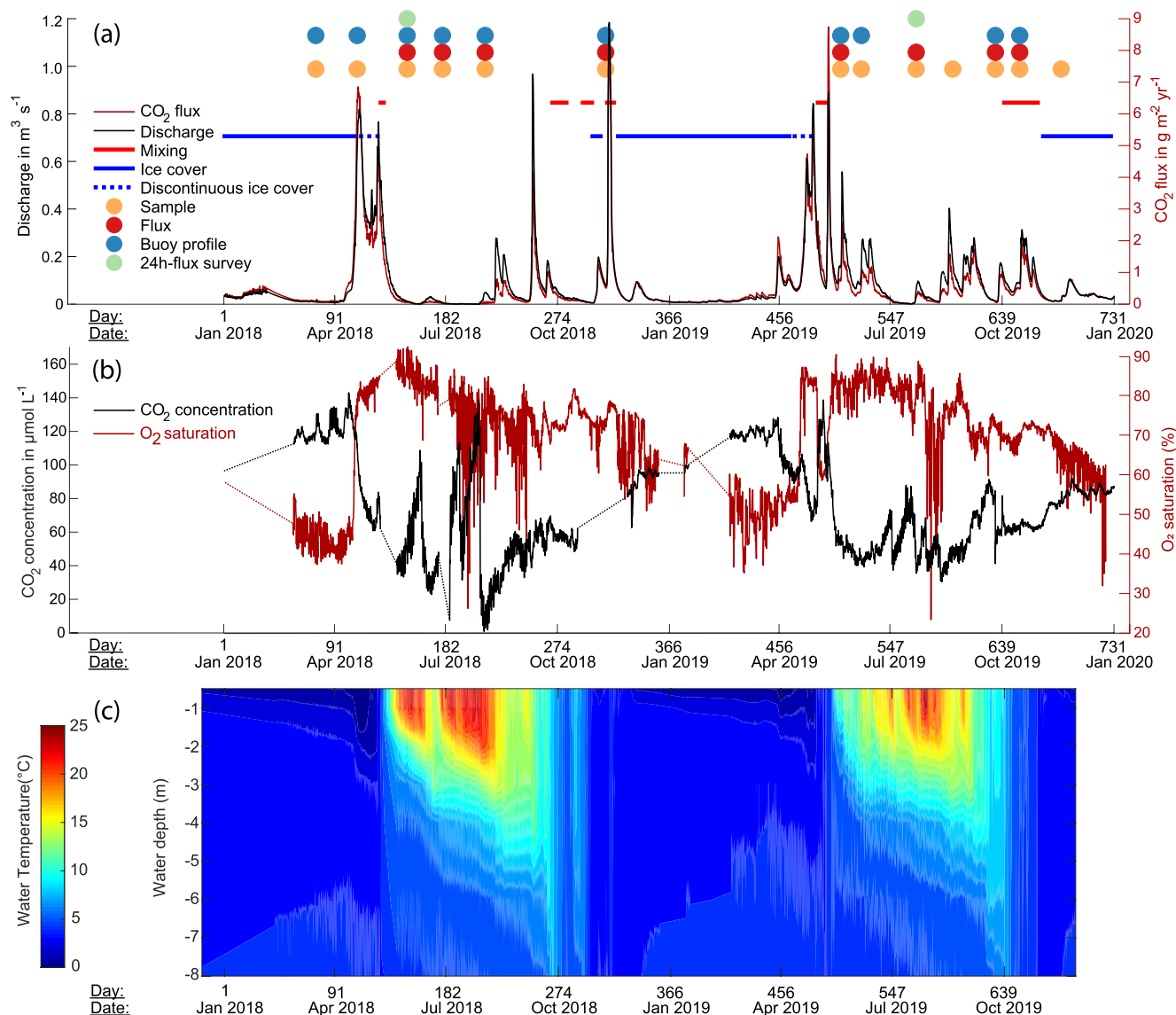


Figure 2. Panel (a), dissolved CO_2 lateral flux (red line) and water discharge (black line) at the lake outlet monitoring station along with the timing of mixing (thick red line) and ice-cover (thick blue line) in Lake Langtjern in 2018 and 2019. Color dots show the dates when sampling for dissolved gases, CO_2 fluxes measurements, dissolved gases profiles and 24-hr-flux surveys were performed. Panel (b), dissolved CO_2 concentration and O_2 saturation. Panel (c), heat map of the water temperature in the lake water column. The ice-covered period was defined as the time from the first complete freezing in autumn until total clearing of ice in spring as proposed by Robertson et al. (1992).

back-flushing (Agilent 7890A, Santa Clara, CA, USA). The GC was equipped with a 20-m wide-bore (0.53 mm) Poraplot Q column operated at 38°C and with He as carrier gas for separation of CH_4 , CO_2 and N_2O from bulk gases. N_2O and CH_4 were measured with an electron capture detector run at 375°C , and a flame ionization detector, respectively. CO_2 and O_2 were measured with a thermal conductivity detector (TCD). Certified standards of CO_2 , N_2O , and CH_4 in He were used for calibration (AGA, Germany), whereas air was used for calibrating O_2 . The analytical error for all gases was lower than 1%. Dissolved gas concentrations were calculated from head-space concentrations using temperature-dependent Henry's law constants provided by (Wilhelm et al., 1977) and the average temperature recorded during the 2-hr equilibration period.

2.6. Carbon Flux Calculations

Carbon fluxes in the East inlet and outlet streams were calculated using measured (bi-hourly or daily) discharge and estimated (bi-hourly or daily) inorganic and organic C concentrations. Over 2017–2019, the bi-hourly DIC concentration at the outlet was calculated from measured pCO₂ sensor data using Equation 1, measured pH and water temperature using standard equilibrium constants (Stumm & Morgan, 1996). In addition, bi-hourly DIC concentration at the outlet over 2015–2019 was also estimated with a Gaussian process regression using lake, inlet, outlet temperature, inlet and outlet water and fDOM levels as well as lake O₂ concentrations as predictors (R² of 0.95–0.97 calibrated and validated against measured CO₂ concentrations from pCO₂ sensor data in 2017–2019; see Supplementary Note 1). Daily TOC concentrations at the outlet and inlet monitoring stations were interpolated with a cubic spline from weekly and monthly measured concentrations, respectively (Figure S3 in Supporting Information S1; as in de Wit et al., 2018). Bi-hourly, CO₂ concentration at the inlet monitoring station (2015–2019) was calculated with a linear regression using discharge as predictor (R² of 0.56 calibrated and validated against measured CO₂ concentrations in 2018–2019; see Figure S2 in Supporting Information S1). All fluxes are reported as g C m⁻² catchment yr⁻¹. For fluxes estimated at the East inlet, an area scaling factor was applied to extrapolated from the East inlet sub-catchment (0.8 km²) to the whole catchment.

Lake diffusive fluxes of CH₄ and N₂O (F_{gas}) at sampling time points (Figure 2) were estimated as follows:

$$F_{gas} = \frac{k_{600}}{\left(\frac{600}{S_{c_{gas}}}\right)^n} ([gas] - [gas]_{eq}) \quad (4)$$

where $S_{c_{gas}}$ is the gas-specific Schmidt number for a given temperature (Wanninkhof, 2014), $n = 2/3$ (Guérin et al., 2007) and $[gas]_{eq}$ the theoretical dissolved gas (CH₄ or N₂O) concentration in equilibrium with atmospheric gas concentration (1.85 ppm for CH₄ and 0.33 ppm for N₂O, Ades et al., 2020) calculated as:

$$[gas]_{eq} = K_{H_{gas}} [gas]_{air} P_{atm} \quad (5)$$

where $K_{H_{gas}}$ is the Henry constant for the given gas adjusted for in-situ temperature (Stumm & Morgan, 1996). Comparison of the magnitude of fluxes reported from different groups of sites was performed with one-tailed t-test.

Yearly lake diffusive emissions of CO₂, CH₄, and N₂O (2015–2019) were estimated by multiplying the average (errors calculated with minimum and maximum estimated fluxes) daily diffusive fluxes measured during ice-free stratified or mixed periods by the number of days when the lake was stratified and mixed, respectively. Other estimates of lake CO₂ diffusive flux were obtained with Equation 2 using bi-hourly CO₂ concentration from the pCO₂ sensor at the outlet, corrected for CO₂ loss between the lake and outlet monitoring station (see Section 3.2), and temperature adjusted k_{CO_2} estimated with Equation 3 from empirically-determined k_{600} (e.g., Cole & Caraco, 1998). Empirical k_{600} models included were the following: $k_{600} = 2.07 + 0.215U_{10}^{1.7}$ (m d⁻¹; Cole & Caraco, 1998), $k_{600} = 0.45U_{10}^{1.64}$ (m d⁻¹; MacIntyre et al., 1995), $k_{600} = 2.51 + 1.48U_{10} + 0.39U_{10}\log_{10} LA$ (m d⁻¹; Vachon & Prairie, 2013), $k_{600} = 0.72U_{10}$ for $U_{10} < 3.7$ m s⁻¹, and $k_{600} = 4.33U_{10} - 13.3$ for $U_{10} \geq 3.7$ m s⁻¹ (cm h⁻¹; bilinear model; Crusius & Wanninkhof, 2003), and $k_{600} = 0.228U_{10}^{2.2} + 0.168$ (cm h⁻¹; power model; Crusius & Wanninkhof, 2003). U_{10} and LA refer to mean wind speed at 10 m in m s⁻¹ (calculated from measured wind speed at 2 m according to Winslow et al., 2016) and lake area in km², respectively.

Yearly lake CH₄ ebullitive fluxes were estimated following two methods: (a) an empirical model expressing CH₄ ebullitive fluxes as a function of mean DOC concentration for lakes within the Northern temperate zone (Fernandes Sanches et al., 2019), and (b) an area- and CH₄ concentration-scaling of ebullitive fluxes reported for three boreal lakes in Québec showing physico-chemical properties that are similar to Langtjern (e.g., DOC, area, mean depth, and chl-*a*; DelSontro et al., 2016). The second estimation of lake CH₄ ebullition ($F_{CH_4}^{Ebul}$) at Langtjern was obtained with the following equation:

$$F_{CH_4}^{Ebul} = \alpha DLA_{3m} f_{CH_4}^{Ebul} \quad (6)$$

where $f_{CH_4}^{Ebul}$ is the average ebullition fluxes reported for three boreal lakes in Québec (0.5–1.5 mmol m⁻² d⁻¹; DelSontro et al., 2016), LA_{3m} is the surface area of Lake Langtjern that is less than 3-m deep (1.5×10^5 m²), D is

the number of ice-free days observed at Lake Langtjern and α is the ratio between the mean observed CH_4 concentration at Langtjern and that from the boreal lakes in Québec (0.25; Rasilo et al., 2015; DelSontro et al., 2016).

Along the aquatic continuum, downstream of lake Langtjern, TOC removal in Lake Krøderen and River Drammenselva (Figure 1a) were estimated from empirical relationships between residence time and TOC decay rate (Catalán et al., 2016). Lake TOC processing for the small lakes within the Langtjern catchment (Figure 1b) was area-scaled from Lake Langtjern TOC processing. Note that this procedure yields a conservative estimate of upstream lake TOC processing since upstream lakes are among the most efficient TOC processors within the boreal landscape (Mattsson et al., 2005). CO_2 evasion from streams in the Langtjern catchment was estimated from mean measured CO_2 concentrations and estimated $k\text{CO}_2$ values for first and second order mountainous streams ($10\text{--}20\text{ m d}^{-1}$; Horgby et al., 2019; Schelker et al., 2016; Ulseth et al., 2019). These $k\text{CO}_2$ values were constrained with estimates from slope, discharge, flow velocity and stream width (Schelker et al., 2016) and are typical values reported for mountainous streams showing similar characteristics, that is, width (0.3–0.6 m), slope (5–15%) and discharge ($0.01\text{--}0.3\text{ m}^3\text{ s}^{-1}$; Horgby et al., 2019; Ulseth et al., 2019). Note that our flux chambers measurements in streams were performed on stream pools and largely underestimate the CO_2 evasion from turbulent stream sections such as small waterfalls. In addition, we compared area-specific annual TOC loads calculated with discharge and TOC concentrations data over various fractions of the Drammenselva river basin to validate the consistency of our regional estimates. Our comparison included TOC loads (a) for the whole river basin, calculated at the mouth of River Drammenselva from the Norwegian river monitoring program (Veitenberg Braaten et al., 2020; Table S6 in Supporting Information S1), (b) for the Tyrifjorden subcatchment (Figure 1a; calculated from down-scaled discharge and average DOC concentrations in Tyrifjorden; Solheim et al., 2020), (c) for the Krøderen subcatchment (Figure 1a; calculated from down-scaled discharge and average DOC concentrations in Krøderen; Solheim et al., 2019) and (d) for the Langtjern catchment calculated with data reported in the present study.

3. Results

3.1. Sensor Data

Daily lake webcam pictures, periodic changes in lake temperature, outlet discharge, and CO_2 concentrations provide sufficient evidence to describe the timing of ice-cover, stratification onset, and mixing events (Figure 2). Over 2015–2019, the average duration of spring and autumn mixing periods were 9.2 ± 3.0 days and 40.4 ± 5.3 days, respectively, while the ice-covered period lasted 142.4 ± 15.3 days. Note that the spring mixing event usually occurs a few days after complete ice-off, that is, when the entire lake surface is free of ice.

3.2. Dissolved Gas Concentrations

The highest CO_2 concentrations at the outlet monitoring station were recorded at the end of the winter (beginning of April) when ice cover was still continuous (Figure 2), then a rapid decrease in CO_2 concentration was observed as the ice cover disappeared. Note that at that time, the lake was still stratified. In 2019, a significant CO_2 peak occurred in May, after the ice off, coinciding with the mixing of the lake. In 2018, the equivalent pCO_2 sensor data were lost due to sensor temporary shutdown. Over the summer (June–August), the CO_2 concentrations remained at a lower level than during winter, experiencing occasional peaks often coinciding with low outlet discharge. And finally, CO_2 concentrations increased again during autumn and steadily throughout winter.

CO_2 , CH_4 , and N_2O concentrations in lake and stream waters at Langtjern varied between 30 and 342 μM , 0.01 and 1.69 μM , and 8 and 14 nM, respectively (Figure 3). These concentrations are typical for boreal surface waters (Kortelainen et al., 2020; Weyhenmeyer, Kortelainen, et al., 2012) although N_2O concentrations are in the lower range which was expected given the low N deposition and high N retention at Langtjern (Kaste et al., 2020).

Dissolved CO_2 and CH_4 concentrations at all sites were always oversaturated, meaning that surface waters at Langtjern are net sources of CO_2 and CH_4 for the atmosphere (Figure 3). By contrast, N_2O concentrations were close to atmospheric equilibrium. Concentrations of the three GHGs were higher in the inlet streams than at the lake sites or by the outlet monitoring stations except during the ice-covered period where concentrations were high at all the measured sites (Figure 3). In addition, CO_2 and N_2O concentrations at the epilimnetic sites were

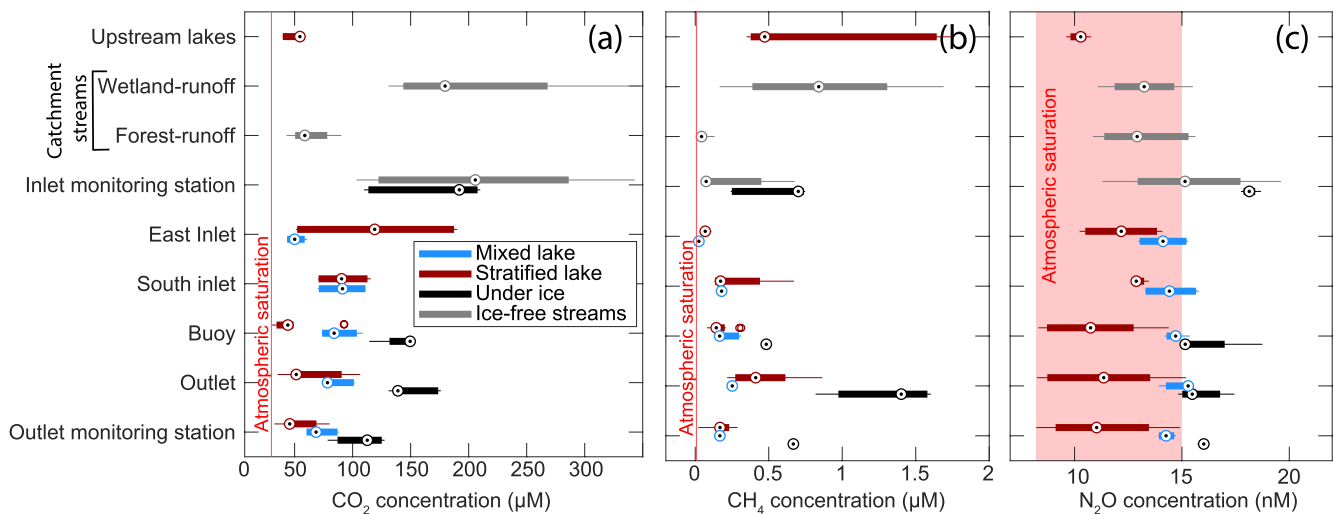


Figure 3. Dissolved greenhouse gas concentration at sampling sites shown in Figure 1. For each boxplot, the central black and white dot indicates the median, and the bottom and top edges of the filled box indicate the 25th and 75th percentiles, respectively. The whiskers extend to the most extreme data points not considered outliers, and the outliers, when present, are plotted individually as empty circles.

higher during mixing periods than when the lake was stratified. No significant difference were observed in dissolved O_2 concentrations among the various sites ($287 \pm 38 \mu\text{M}$), except for the East inlet stream ($322 \pm 37 \mu\text{M}$).

Concentrations of dissolved gases were lower at the lake outlet monitoring station (510 m.a.s.l., ca 80 m downstream; Figure 1c) than at the lake outlet (516 m.a.s.l.), except for O_2 which increased to saturation (Figure 4a). CO_2 and CH_4 concentrations showed a decrease of 10%–15% and 30%–80%, respectively. This is consistent with the O_2 -poor, CO_2 - and CH_4 -rich lake water being reaerated from the outlet downstream to the monitoring station (6 m elevation difference, and about 80 m distance) as a consequence of stream turbulence, and CH_4 being more volatile than CO_2 .

Dissolved CO_2 , N_2O , and CH_4 concentrations showed a distinct vertical distribution over the water column as shown in Figure 4. Under ice, CO_2 concentrations were slightly larger below 2 m depth than at the surface while CH_4 showed variable patterns and N_2O was mainly constant. During stratification, CO_2 concentrations below 2 m depth were significantly larger than at the surface (P -value < 0.001 for CO_2 and < 0.01 for N_2O) while CH_4 concentrations showed the opposite pattern, higher concentrations at the surface (P -value < 0.001). During mixing,

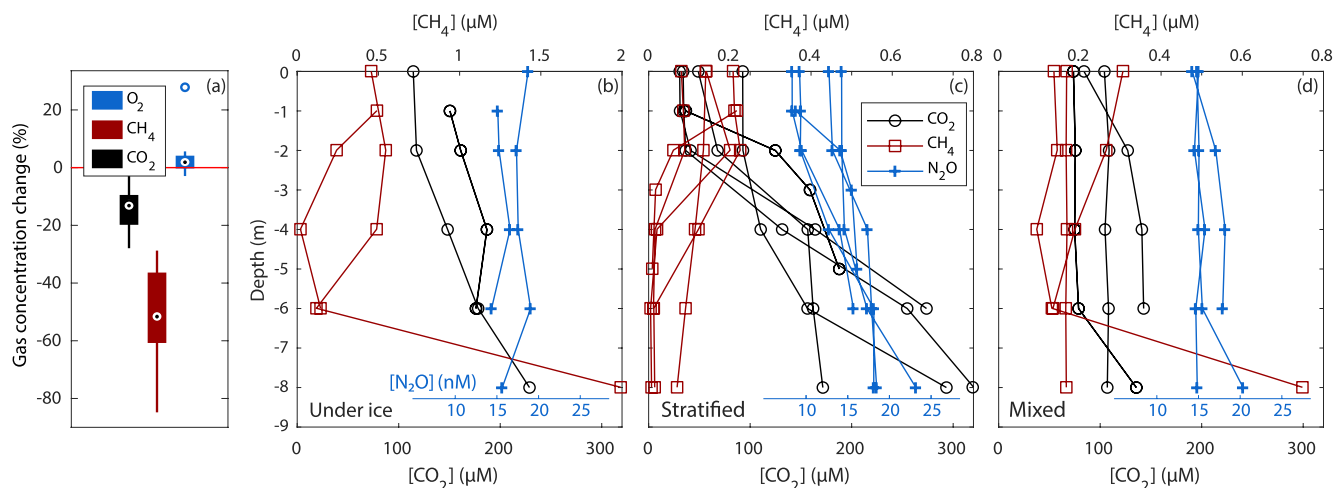


Figure 4. Change in dissolved gas concentrations from outlet to outlet monitoring station (a) and profiles of mean dissolved CO_2 , N_2O , and CH_4 concentrations at the lake buoy under ice (b), stratification (c) and mixing (d). Error bars, representing standard deviation of duplicate or triplicate samples, were smaller than the symbols.

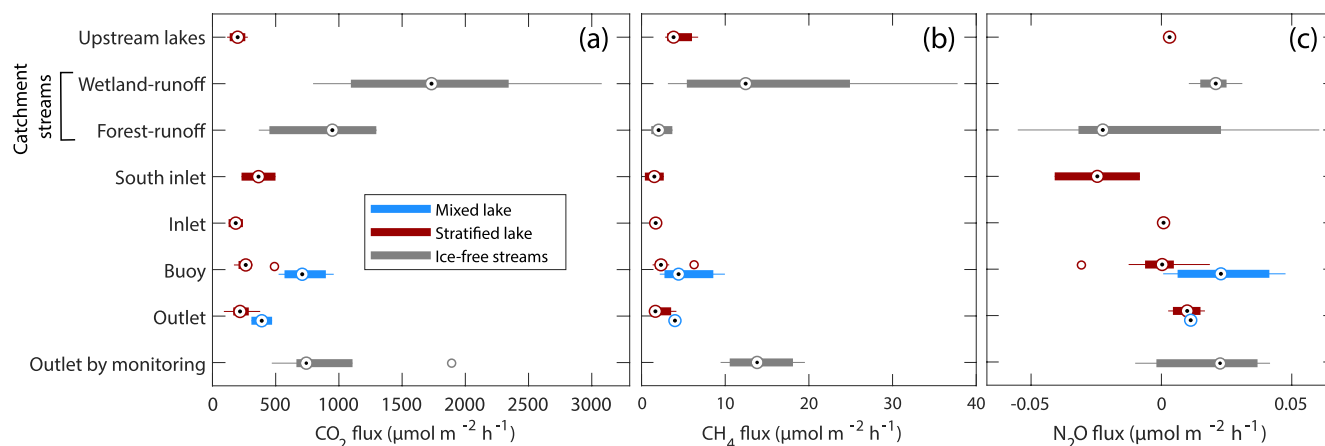


Figure 5. Greenhouse gas fluxes at the water surface at sampling sites shown in Figure 1. For each boxplot, the central black and white dot indicates the median, and the bottom and top edges of the filled box indicate the 25th and 75th percentiles, respectively. The whiskers extend to the most extreme data points not considered outliers, and the outliers, when present, are plotted individually as empty circles.

the concentrations were relatively homogenous over the whole water column. Only two exceptions were observed for CH_4 in two deep samples near the lake bottom.

3.3. Greenhouse Gas Evasion Fluxes

Box plots of CO_2 , CH_4 , and N_2O diffusive fluxes are shown in mole units in Figure 5 for various lake and stream sites to allow for comparison between the three gases. Similar flux magnitudes were obtained for all lake sites during the stratified (243 ± 97 , 2.6 ± 1.6 and $0.00 \pm 0.01 \mu\text{mol m}^{-2} \text{hr}^{-1}$ for CO_2 , CH_4 , and N_2O , respectively) and the mixed (594 ± 223 , 4.9 ± 2.6 and $0.02 \pm 0.02 \mu\text{mol m}^{-2} \text{hr}^{-1}$ for CO_2 , CH_4 , and N_2O , respectively) periods, respectively. Fluxes from the lake sites during mixing were significantly larger (P -value < 0.001 for CO_2 and < 0.05 for CH_4 and N_2O) than during thermally stratified conditions. Stream CO_2 effluxes ($1,196 \pm 715 \mu\text{mol m}^{-2} \text{hr}^{-1}$) were significantly larger than those from lake sites during mixing (P -value = 0.048) or stratification (P -value < 0.001). For CH_4 , fluxes reported from streams ($8.9 \pm 10.0 \mu\text{mol m}^{-2} \text{hr}^{-1}$) and lake sites during mixing were not significantly different, but both were significantly larger than fluxes from lake sites during stratification (P -values of 0.007 and 0.016, respectively). In addition, wetland-fed streams showed significantly higher (P -values of 0.012 and 0.023) CO_2 ($903 \pm 448 \mu\text{mol m}^{-2} \text{hr}^{-1}$) and CH_4 ($4.5 \pm 4.0 \mu\text{mol m}^{-2} \text{hr}^{-1}$) fluxes than other streams ($1,780 \pm 788$ and $16.0 \pm 12.4 \mu\text{mol m}^{-2} \text{hr}^{-1}$ for CO_2 and CH_4 , respectively). For N_2O fluxes, no significant difference was found between stream and lake sites, and only fluxes from wetland-runoff streams and the lake, when mixed, showed N_2O fluxes significantly larger than zero (P value < 0.01). Overall, we present lower CO_2 evasion fluxes than those reported in similar boreal lakes in Sweden which is consistent with higher DOC concentrations at these sites (e.g., Denfeld et al., 2018; Heiskanen et al., 2014).

Extrapolation from flux chamber measurements over 2018–2019 yielded a yearly diffusive CO_2 flux of $1.3 \pm 0.6 \text{ g C m}^{-2} \text{ catchment yr}^{-1}$ from Lake Langtjern (Figure 6). While estimations of CO_2 diffusion from high-frequency measurements of pCO_2 at the lake outlet, wind and water temperature over 2015–2019 ranged between 1.4 ± 0.2 (power k_{600} model from Crusius & Wanninkhof, 2003) and $12.9 \pm 0.6 \text{ g C m}^{-2} \text{ catchment yr}^{-1}$ (k_{600} model from Vachon & Prairie, 2013). The other k_{600} models yielded intermediate values of 1.5 ± 0.2 (bilinear k_{600} model from Crusius & Wanninkhof, 2003), 3.2 ± 0.2 (k_{600} model from MacIntyre et al., 1995), and $7.7 \pm 0.5 \text{ g C m}^{-2} \text{ catchment yr}^{-1}$ (k_{600} model from Cole & Caraco, 1998). Yearly diffusive CH_4 emissions were $0.01 \pm 0.01 \text{ g C m}^{-2} \text{ catchment yr}^{-1}$, while ebullitive CH_4 fluxes were estimated to range between 0.02 ± 0.01 (calculated from mean DOC concentrations; Fernandes Sanches et al., 2019) and $0.03 \pm 0.01 \text{ g C m}^{-2} \text{ catchment yr}^{-1}$ (scaling of ebullitive fluxes of DelSontro et al., 2016). Diffusion of N_2O was estimated at $0.9 \pm 6.2 \mu\text{mol m}^{-2} \text{ catchment yr}^{-1}$. Finally, accounting for their radiative forcing, that is, 25 and 298 that of CO_2 for CH_4 and N_2O , respectively, CH_4 emissions account for 31%–41% of total lake radiative forcing, while N_2O emissions were negligible.

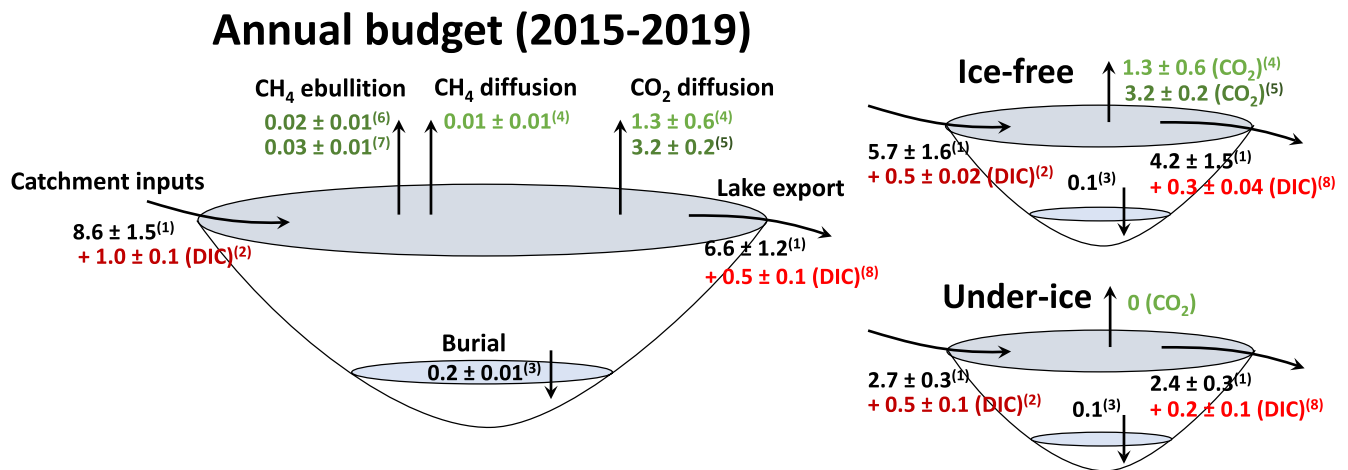


Figure 6. Revisited Langtjern C budget. All rates are in g C m⁻² catchment yr⁻¹. (1) TOC flux from measured discharge and TOC concentrations. (2) DIC flux from linearly regressed CO₂, average pH and measured discharge. (3) Burial rate from de Wit et al. (2018). (4) Average CO₂ and CH₄ diffusive fluxes measured with chambers in 2018–2019. (5) CO₂ diffusive flux from Gaussian Process regression (CO₂) and empirical kCO₂ models over 2015–2019. (6) CH₄ ebullition estimated from DOC concentrations (Fernandes Sanches et al., 2019). (7) CH₄ ebullition estimated from area- and CH₄ concentration-scaling of ebullitive fluxes reported by DelSontro et al. (2016) (8) DIC flux from Gaussian Process regression (CO₂), measured pH and discharge.

3.4. Lateral C Fluxes Based on Monitoring

Our monitoring and sensor data allow to calculate TOC as well as DIC fluxes from catchment to lake and at the lake outlet over 2015–2019 (Figure 6). Lake DIC (0.5 ± 0.1 g C m⁻² catchment yr⁻¹) and TOC (6.6 ± 1.2 g C m⁻² catchment yr⁻¹) exports were substantially lower than DIC (1.0 ± 0.1 g C m⁻² catchment yr⁻¹) and TOC (8.6 ± 1.5 g C m⁻² catchment yr⁻¹) catchment inputs, respectively. Hence, the lake acts as a barrier for organic and inorganic carbon during downstream transport due to TOC mineralization and burial in sediment as well as CO₂ degassing. The net lake organic C removal can be estimated by subtracting lake exports to catchment input fluxes. We estimate that 2.0 ± 0.5 g C m⁻² catchment yr⁻¹ of organic C, is processed by the lake over 2015–2019 representing on average 25% of the incoming organic C.

3.5. C Processing Based on Lake DOC Modeling

The calibrated GOTM-Selma-DOMCAST model predicted temperature, dissolved O₂, and DOC concentrations that were in overall good agreement with observed data over the calibration and validation periods (Tables S2 and S3, Figure S2 in Supporting Information S1). The bottom O₂ and outlet DOC concentrations were accurately reproduced by the model as evidenced by Nash–Sutcliffe model efficiency coefficients (NSE) of 0.4 or higher and R² values of 0.5 or higher (Tables S2 and S3 in Supporting Information S1). In contrast, surface O₂ concentrations were modeled with less success, although the main seasonal variations were captured by the model. The GOTM-Selma-DOMCAST model reproduced O₂ and DOC concentrations at Langtjern with a lower degree of accuracy than MyLake as reported for O₂ or DOC by Couture et al. (2015) and de Wit et al. (2018), respectively. MyLake was calibrated for one variable at a time, either O₂ (Couture et al., 2015) or DOC (de Wit et al., 2018), while GOTM-Selma-DOMCAST was calibrated against both variables simultaneously. However, the GOTM-Selma-DOMCAST model produced realistic concentrations for DOC and O₂ which gives some additional confidence in the DOC processing rates computed by the model.

The modeled lake DOC removal was dominated by oxic respiration and flocculation, while denitrification and photo-mineralization were negligible (Table S4 in Supporting Information S1). The total lake DOC removal was on average 0.3 g C m⁻² catchment yr⁻¹ over 2015–2019 which is consistent with previous estimates over 1986–2015 at the same study site (0.4 g C m⁻² catchment yr⁻¹; de Wit et al., 2018). The estimated rate is equivalent to a decay rate of 0.04 years⁻¹ and falls within the lower range reported for inland waters (Catalan et al., 2016). This DOC removal rate is significantly lower than mass-balance estimated lake TOC removal (2.0 ± 0.5 g C m⁻² catchment yr⁻¹, this study; 0.6 ± 0.1 g C m⁻² catchment yr⁻¹, de Wit et al., 2018). This discrepancy is discussed below.

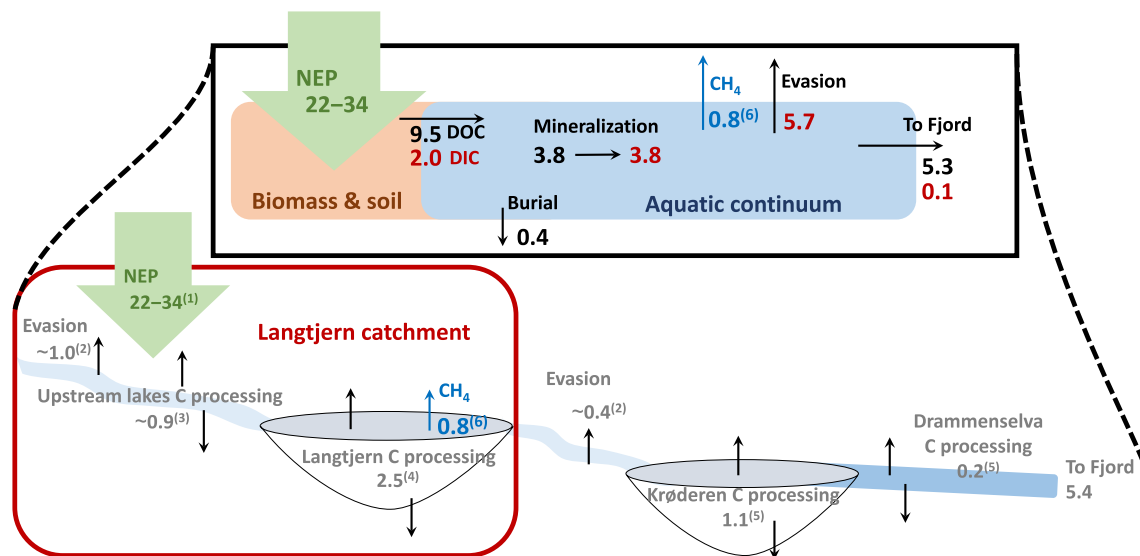


Figure 7. Fate of the organic C accumulated in the Langtjern catchment at the regional scale, from headwater to fjord. All rates are in g C m^{-2} catchment yr^{-1} . (1) Forest and soil C accumulation rates (de Wit et al., 2015). (2) Stream CO_2 evasion fluxes estimated with average kCO_2 for mountainous streams (Schelker et al., 2016; Ulseth et al., 2019) and average measured concentrations in Langtjern streams. (3) Downscaling of Lake Langtjern TOC processing. (4) Rates from Figure 6. (5) TOC removal estimated with water residence time after Catalan et al. (2016). (6) CH_4 diffusion and ebullition in CO_2 equivalents.

3.6. C Processing Rates Along the Aquatic Continuum

Small lakes in the southern part of the Langtjern catchment totalize 0.1 km^2 (Figure 1b). Assuming similar TOC processing rates as in Lake Langtjern, area-scaling of Langtjern TOC processing yields 0.9 g C m^{-2} catchment yr^{-1} , including 0.1 g C m^{-2} catchment yr^{-1} of organic C burial, in these small lakes. We further estimate, based on kCO_2 for first order mountainous streams and measured stream CO_2 concentrations, that 0.9 g C m^{-2} catchment yr^{-1} CO_2 evades from streams before reaching Lake Langtjern. In addition, based on estimated kCO_2 values, stream water exported from Langtjern (516 m above sea level) reaches atmospheric equilibrium before entering Lake Krøderen (133 m above sea level). Hence, we estimate that, out of the 0.5 g C m^{-2} catchment yr^{-1} of DIC exported from Langtjern (corresponding to a mean DIC concentration of $80 \mu\text{M}$ vs. atmosphere equilibrium around $20 \mu\text{M}$), 0.4 g C m^{-2} catchment yr^{-1} evades as CO_2 to the atmosphere before reaching Lake Krøderen.

Within Lake Krøderen, we estimated a TOC decay rate of 0.17 years^{-1} from its water retention time of 0.36 years (Catalan et al., 2016) which implies a TOC removal of 1.1 g C m^{-2} catchment yr^{-1} , of which 0.1 g C m^{-2} catchment yr^{-1} is estimated to be buried based on the ratio between mineralization and burial reported for Langtjern. We finally estimate a TOC decay rate of 0.04 years^{-1} (Catalan et al., 2016) for Drammenselva based on a 12-day water travel time corresponding to a TOC removal of 0.2 g C m^{-2} catchment yr^{-1} . All fluxes are summarized in Figure 7.

Finally, riverine TOC loads from Drammenselva river basin ($17,034 \text{ km}^2$) were $2.1 \text{ tons C yr}^{-1} \text{ km}^{-2}$ over 2016–2019, while loads for the Krøderen ($5,092 \text{ km}^2$) and Tyrifjorden ($9,967 \text{ km}^2$) subcatchments were 1.4 and $2.1 \text{ tons C yr}^{-1} \text{ km}^{-2}$, respectively. This is consistent with the fact that TOC export from Langtjern catchment ($6.6 \text{ tons C yr}^{-1} \text{ km}^{-2}$) are larger than the average TOC export from the whole Drammenselva river basin. Indeed, larger TOC exports from forested subcatchments in the lower part of the river basin are needed to counterbalance the relatively low TOC loads from Krøderen subcatchment.

4. Discussion

4.1. Key Sources, Transport, and Processing of C and GHG

The import and export of C into and from Lake Langtjern show distinctive seasonal patterns driven by changes in discharge and concentrations of the different C species. While the highest DIC fluxes are usually observed in spring during ice melt, as a result of high discharge and continuous accumulation of CO_2 in the ice-covered

lake in winter (Figure 2), the highest TOC fluxes are usually observed during autumn when both, discharge and concentrations, are high (Figure 2a and Figure S3 in Supporting Information S1). The inorganic carbon fluxes, including CO₂ evasion, are driven, to a larger extent than TOC fluxes, by physical processes as already acknowledged (e.g., Denfeld et al., 2018; Karlsson et al., 2013). Indeed, the ice cover and stratification act as barriers for CO₂ evasion, as evidenced by high surface CO₂ concentrations under ice (Figure 3), and higher CO₂ diffusive fluxes during mixing than during stratification (Figure 4). In addition, the elevated CO₂ concentrations observed in May 2019 coinciding with lake mixing are interpreted to represent hypolimnetic CO₂ accumulated during the winter which is consistent with findings from a small boreal lake in Sweden (Denfeld et al., 2015).

The continuous accumulation of CO₂ in the lake under ice indicates that the sediment or the water-column is a significant source of CO₂ for the lake. While some of the CO₂ accumulated under-ice may originate from the catchment (Denfeld et al., 2015), the fact that CO₂ concentrations consistently increase throughout the winter while O₂ concentrations decrease despite the very low inflows support a strong internal CO₂ production (Figure 2b). In addition, under ice or during stratification, hypolimnetic waters always had higher CO₂ concentrations than epilimnetic waters (Figures 4b and 4c). Interestingly, CH₄ did not accumulate in the hypolimnion during stratified periods, and the highest concentrations in the stratified lake were observed in the surface waters (Figure 4c). Only two deep water samples exhibited relatively high CH₄ concentrations suggesting some CH₄ outflux from the hypolimnetic sediments (Figures 3b–3d). However, either the hypolimnetic sediment CH₄ export is too low, or CH₄ oxidation is too high to build up a significant CH₄ stock in the hypolimnion. The catchment did not seem to be a major source of CH₄ for the lake, as lower concentrations were reported at both inlets than at the buoy or outlet (Figure 3). In fact, CH₄ concentrations dropped within the stream, including a small waterfall, connecting the inlet monitoring station to the east inlet (Figure 3). This is consistent with the expected high piston velocity in steep stream sections including small waterfalls (Natchimuthu, Wallin, et al., 2017). Hence, most of the CH₄ sampled at the buoy and at the outlet is thought to originate from littoral sediment (e.g., Bartosiewicz et al., 2016) and possibly from pelagic production (Bogard et al., 2014). The magnitude of ebullition, estimated to export two to three times more CH₄ than diffusion, further highlights the key role of littoral sediments for CH₄ evasion from Lake Langtjern. Indeed, littoral sediments, that is, shallower than 3 m (DelSontro et al., 2016), represent 64% of the lake bottom. Note, however, that ebullitive fluxes were not measured but originate from the scaling of ebullitive fluxes reported in the literature, and should therefore be taken with caution.

N₂O is mainly produced during aerobic nitrification and anaerobic denitrification (Butterbach-Bahl et al., 2013). The intensity of lake N cycling, involving nitrification and denitrification, and by extension of N₂O production is directly depending on nitrate concentrations. In fact, nitrate concentrations explained as much as 78% of the variation of the seasonal mean N₂O concentrations across a large set of Finnish boreal lakes (Kortelainen et al., 2020). At Langtjern, given the low nitrate concentration (0.2 μM; Couture et al., 2015), N₂O production is expected to be low. In fact, most of the measured N₂O concentrations at Langtjern were close to atmospheric equilibrium (Figure 3) and most measured diffusive N₂O fluxes were close to zero (Figure 4). Interestingly, significant N₂O effluxes were only observed from the lake, when mixed, and from wetland-runoff streams. In addition, N₂O concentrations were always higher in the hypolimnion than in the epilimnion, when the lake was stratified, suggesting that the hypolimnetic sediment and/or waters are the main source of lake N₂O. These findings are consistent with the fact that wetlands and hypolimnetic waters often include an aerobic-anaerobic boundary, where N turnover through denitrification and nitrification is likely persistent. Hence, under low nitrate conditions, the repetitive transfer of N from aerobic to anaerobic environments might sustain significant, albeit low, N₂O production. We further suggest that this process leads to Lake Langtjern being a net source of N₂O for the atmosphere.

A mass balance of the inorganic carbon fluxes into and from the lake shows that the catchment is a significant source of DIC, which is consistent with other studies (e.g., Natchimuthu, Sundgren, et al., 2017). However, the stream DIC import is too small to account for both lake CO₂ evasion and export through the discharge at the outlet (Figure 6). Diffuse below-ground water flows are poorly constrained which can lead to an under-estimation of the TOC, DIC and CH₄ inputs to the lake (Einarsdottir et al., 2017). However, these should not play a major role since soils at Langtjern are shallow (de Wit et al., 2014). Note also that DIC originating from weathering reactions are assumed to be negligible as the geology at Langtjern consists of felsic gneisses and granites. Hence, in-lake CO₂ production is needed to be able to account for the lake CO₂ efflux to the atmosphere and through the outlet. Note that annual CO₂ evasion estimated from flux chamber data is most likely underestimated (Figure 2) because CO₂ efflux at ice-off was not represented in our measurements although it can account for 11%–55% of

annual evasion in Nordic lakes (Denfeld et al., 2018; Karlsson et al., 2013). In fact, all the other estimates, based on various k_{600} models and high-frequency $p\text{CO}_2$ measurements at the lake outlet (see Section 3.3), yielded higher lake CO_2 diffusive fluxes ranging from 1.4 to 12.9 g C m^{-2} catchment yr^{-1} . The disparity between the estimations of CO_2 diffusion likely arises from the fact that under low wind speed (i.e., $<2 \text{ m s}^{-1}$), as it is the case most of the time at Langtjern, CO_2 diffusion is likely driven by other processes than wind-induced turbulence that are not represented in the k_{600} models (MacIntyre et al., 2010; Vachon & Prairie, 2013). While CO_2 evasion fluxes above 7 g C m^{-2} catchment yr^{-1} (k_{600} model from Cole & Caraco, 1998, and Vachon & Prairie, 2013) are unlikely for the same reasons as mentioned above, fluxes between 1.4 and 3.2 g C m^{-2} catchment yr^{-1} (k_{600} model from Crusius & Wanninkhof, 2003, and MacIntyre et al., 1995) would be consistent with other C fluxes at Langtjern, for example, lake TOC removal of 2.0 g C m^{-2} catchment yr^{-1} (see Section 3.4; Figure 6). Note that for all CO_2 diffusive fluxes, we assumed no CO_2 evasion during the ice-covered period. For the above-mentioned reasons, our C fluxes into Lake Langtjern and C processing rates in the lake are likely conservative estimates, whereas estimates of TOC and DIC export at the lake outlet are fairly unbiased.

In summary, inorganic carbon fluxes estimated from floating CO_2 flux chambers, high-frequency $p\text{CO}_2$ sensor and targeted water sampling show that CO_2 production in Lake Langtjern is significant, as evidenced, inter alia, by under-ice CO_2 accumulation, high CO_2 effluxes and high lateral DIC export during lake mixing. While DIC can originate from plant respiration (autochthonous CO_2) and microbial mineralization of soil organic matter and TOC (allochthonous) in the catchment, the CO_2 produced in the lake is mainly derived from TOC mineralization in the sediment and water column. To clarify the role of these inorganic carbon fluxes for the C cycle of Lake Langtjern, the relative contributions of soil export versus in-stream and in-lake production to CO_2 evasion and DIC lateral export is ultimately needed. Only aquatic inorganic carbon fluxes contributing to long-term soil C depletion in the catchment, for example, in-lake CO_2 production from soil-derived DOC, ultimately impact atmospheric CO_2 and the C cycle. Inorganic carbon fluxes related to plant respiration or degradation of photosynthates are of less relevance for the land C sink. In that regard, the determination of stable C isotopes is a major asset to relate the measured DIC to its original sources (Campeau et al., 2017) and should be included in future sampling efforts.

4.2. Lake Langtjern C Budget

Lake Langtjern TOC removal can be estimated based on various flux estimates reported in this study including empirical TOC flux mass balances, modeled DOC processing rates and lake CO_2 evasion. As discussed above, inorganic carbon fluxes are likely conservative, and a mass balance of the DIC fluxes and CO_2 evasion would thus yield a conservative estimate of lake TOC processing. In addition, we noted that GOTM-Selma-DOMCAST gave DOC processing rates lower than those estimated with the empirical TOC fluxes mass balance (see Section 3.5). The underestimation of the DOC processing rates by GOTM-Selma-DOMCAST is partly an artifact of the calibration procedure in which each concentration value was weighted equally, thereby down-weighting the influence of relatively rare high-flow events (de Wit et al., 2018). In addition, GOTM-Selma-DOMCAST tends to overestimate DOC concentrations in summer (Figure S2 in Supporting Information S1) which would induce a significant underestimation of the DOC removal since 40% of the annual DOC exports occurs in summer (May–August). Hence, we submit that the lake TOC removal calculated from the empirical mass balance is the most robust estimation.

The lake TOC removal, as estimated with the TOC flux mass balance, was $2.0 \pm 0.5 \text{ g C m}^{-2}$ catchment yr^{-1} over 2015–2019. Considering that 0.2 g C m^{-2} catchment yr^{-1} is buried in the lake sediment, as constrained by the measured sediment accumulation rate (de Wit et al., 2018), in-lake TOC mineralization reaches $1.8 \pm 0.5 \text{ g C m}^{-2}$ catchment yr^{-1} . The mass balance of lake DIC fluxes yields a conservative estimate of $0.8 \pm 0.5 \text{ g C m}^{-2}$ catchment yr^{-1} , which is consistent with the lake TOC removal considering that we underestimate lake CO_2 evasion, as discussed above. Figure 6 further shows that about 86% of the TOC processing occurs during the ice-free period which is in line with the fact that bacterial metabolism represents the main TOC loss since it is enhanced by higher water temperatures (Kraemer et al., 2017) and exposure of DOC to sunlight (Cory et al., 2014).

Our estimation of lake TOC removal at Langtjern over 2015–2019 is larger than our previous estimate of 0.6 g C m^{-2} catchment yr^{-1} over 1986–2015 (de Wit et al., 2018). This difference is mainly related to the 2015–2019 catchment TOC inputs ($8.6 \pm 1.5 \text{ g C m}^{-2}$ catchment yr^{-1}) being larger than those estimated over 1986–2015 ($7.3 \pm 1.8 \text{ g C m}^{-2}$ catchment yr^{-1}), and can partly be explained by changes in precipitation (e.g., de Wit,

Ledesma, & Futter, 2016; de Wit, Valinia, et al., 2016), with the unusually wet years 2015 and 2019 with 1,028 and 1,078 mm, respectively. In addition, the updated estimation of inlet discharge (see Section 2.2; Table S5 in Supporting Information S1) yielded higher inlet discharge than previously estimated.

In summary, Lake Langtjern removed 23% of the incoming TOC, 21% through mineralization and 2% through burial, over 2015–2019 which is similar to the estimates for a small Swedish lake (Chmiel et al., 2016). This TOC processing rate is equivalent to a DOM decay rate of 0.21 yr^{-1} which is within the reported range for decay rates in inland waters considering the average water residence time (mean 0.23 yr^{-1} ; Catalan et al., 2016).

4.3. Regional C Budget

Determining the fate of the exported catchment C, that is, long term burial versus reemission to the atmosphere, is essential for the assessment of landscape C budgets. In particular, large uncertainties remain regarding the C fraction transported laterally along the aquatic continuum from mountain to sea and its significance compared to the land C sink (Ward et al., 2017). Understanding OM processing rates and water residence times allowed us to estimate the fate of exported OC from the Langtjern catchment and to present the lake C budget in a regional context (Figure 7). This provides a first assessment of the role of the aquatic continuum in reducing the land C sink in a typical Norwegian catchment.

The Langtjern catchment is part of the forested land in the Drammenselva river basin (Figure 1a) which is part of the Skagerrak drainage area for which NEP (accumulation of C in biomass and soils, corrected for extractions from forest harvest, averaged over all land cover types including forests, peatlands and mountain areas) was estimated to be $28.4 \text{ g C m}^{-2} \text{ yr}^{-1}$ (de Wit et al., 2015). Land cover in the Skagerrak river basin is representative of the Langtjern catchment (ca 73% of forest), where Langtjern is at the low-productivity range of forest types in southern Norway, suggesting that NEP in Skagerrak is representative of NEP at Langtjern, with an uncertainty interval of 20% (derived from the variation in forest C uptake). This yields a NEP estimate of $28(\pm 20\%) \text{ g C m}^{-2} \text{ catchment yr}^{-1}$ for the Langtjern catchment. Most of the CO_2 evading from small streams is coming from soils or groundwater (Hotchkiss et al., 2015) which complicates the determination of its primary origin, and its link to the land C sink (Campeau et al., 2017). Hence, we excluded stream CO_2 evasion in our assessment thereafter yielding conservative estimates of C evasion. The effective TOC lateral flux reached $9.5 \text{ g C m}^{-2} \text{ catchment yr}^{-1}$ representing 28%–42% of the annual NEP, of which $4.2 \text{ g C m}^{-2} \text{ catchment yr}^{-1}$ was processed before reaching the fjord (Figure 7). TOC mineralization represents $3.8 \text{ g C m}^{-2} \text{ catchment yr}^{-1}$ and 11%–17% of NEP which is consistent with other estimates (Butman et al., 2016; de Wit, Ledesma, & Futter, 2016; de Wit, Valinia, et al., 2016; Öquist et al., 2014; Wallin et al., 2018) while burial only reached $0.4 \text{ g C m}^{-2} \text{ catchment yr}^{-1}$. Hence, at least 40% of the TOC exported from the Langtjern catchment was mineralized before reaching the fjord, likely more if some of the DIC exported originated from in-stream TOC mineralization. In addition, we estimate that at least 68% of the TOC mineralization takes place in the Langtjern catchment (Figure 7) emphasizing the role of headwaters as processors of TOC.

The fate of the remaining laterally transported TOC in the fjord remain to be quantified. Nevertheless, the comparison of the 2016–2019 TOC loads from Drammenselva ($2.1 \text{ g C m}^{-2} \text{ catchment Drammenselva yr}^{-1}$; calculated from Table S6 in Supporting Information S1) and the organic C accumulation rate in Drammensfjord (Huguet et al., 2007; Smith et al., 2015) yields a burial efficiency of 4%–5%, meaning that $5.1 \text{ g C m}^{-2} \text{ catchment yr}^{-1}$ from Langtjern would reach the greater Oslofjord and eventually the open ocean.

The present regional budget is the first assessment of the fate of C exported from a typical boreal headwater catchment in Norway along the aquatic continuum and is prone to uncertainties. While the TOC removal in Lake Langtjern is well constrained highlighting the combined value of long-term monitoring, high-frequency sensor data and targeted sampling campaigns, the estimation of C processing upstream and downstream of Lake Langtjern are derived from shorter time series and a limited number of sampling campaigns. Hence future sampling effort should focus on gathering more frequent and more spatially explicit data on C processing along the aquatic continuum. Nevertheless, our finding that TOC processing primarily occurs in headwaters along the aquatic continuum is in agreement with a study from Sweden showing that organic C loss follows an exponential decay from headwater to coast (Weyhenmeyer, Fröberg, et al., 2012). Some uncertainty also lies in the magnitude of TOC burial along the whole continuum. TOC burial in Lake Langtjern sediment is constrained through modeling by the measured sediment accumulation rate (de Wit et al., 2018). This accumulation rate has been derived from one

representative sediment core accounting for sediment focusing (de Wit et al., 2018). The main uncertainty resides in the fact that we applied the relative partitioning between TOC mineralization and burial at Lake Langtjern to estimate TOC burial in Lake Krøderen. The resulting uncertainty can only be resolved by measuring sediment accumulation rate in Lake Krøderen sediments. However, even if TOC burial would have been underestimated in the present budget by a factor of two, it would not discredit our finding that over 67% of the TOC mineralization occurs in the headwater catchment and that at least 35% of the laterally transported TOC is mineralized before reaching the fjord.

4.4. Implications for the Land C Sink

Understanding the ultimate fate of the C fixed by photosynthesis on land is key for quantifying the net land C sink, that is, NEP, and evaluate the feedback effect of the aquatic continuum on the climate system. Over 35% of the TOC exported from the Langtjern catchment is mineralized representing a NEP reduction of 11%–17%. Even if CH₄ and N₂O evasion are negligible compared to TOC and CO₂ in terms of molar fluxes, considering that their radiative forcings are respectively 25 and 300 times larger than that of CO₂, can further reduce NEP. Lake Langtjern CH₄ evasion alone would account for another $0.8 \pm 0.4 \text{ g C m}^{-2} \text{ catchment yr}^{-1}$, which is equivalent to ~3% of NEP. Given that smaller aquatic systems emit relatively more CH₄ than larger systems (DelSontro et al., 2018; Holgerson & Raymond, 2016), CH₄ evasion from upstream lakes in Langtjern catchment likely contribute to further reducing NEP, while CH₄ emissions from downstream Lake Krøderen and Drammenselva might be less important. For N₂O, it is possibly the opposite pattern as nitrate concentration has been showed to be the main driver of N₂O emissions and it is increasing downstream toward Drammenselva mouth, albeit still at low levels (Veitenberg Braaten et al., 2020). Nevertheless, within the Langtjern catchment, N₂O emissions are negligible compared to NEP.

Considering that the overall water residence time for Langtjern, from headwater to fjord, is in the order of 0.7 years including only ~0.25 years within the Langtjern catchment (excluding soil water retention), we submit that mountainous boreal catchments are fast-responding ecosystems. Hence small headwater lakes and streams have a disproportionate, that is, prominent role in the C cycle compared to their larger downstream counterparts, both in terms of magnitude and response time. In summary, we estimate that at least 10%–14% of the NEP is directly reduced through TOC processing and GHG evasion in the Langtjern catchment, within 2–4 km from photosynthetic fixation and over ~3 months time, while a remaining 4%–6% of the NEP is further reduced downstream over a longer time period.

5. Conclusions

Our catchment C budget revealed that mineralization removed 21% of the incoming TOC in Lake Langtjern sustaining high CO₂ efflux and lateral DIC export, as well as some CH₄ evasion through diffusion and ebullition. The lake was also a net source of N₂O, mainly originating from the hypolimnion, although N₂O fluxes were negligible compared to CO₂ and CH₄, even when accounting for their respective radiative forcings. Most of the TOC processing, over 67% of the sum of TOC processing along the aquatic continuum from headwater to fjord, occurred over relatively short timescales in the Langtjern catchment highlighting the prominent role of headwater lakes and streams in the C cycle. Up to 14% of the land C sink at Langtjern is estimated to be directly reduced within the catchment through mineralization and GHG evasion. This estimate is likely conservative since we ignored stream CO₂ evasion. Additional sampling works is required to elucidate the precise origin of the measured stream DIC, for example, through the measurement of stable isotopes (Campeau et al., 2017), and clarify its impact on the C cycle. In addition, the future significance of headwater catchments as processors of terrestrial C remains to be investigated more closely considering that browning of inland waters will be further promoted by a wetter future climate (de Wit, Ledesma, & Futter, 2016; de Wit, Valinia, et al., 2016).

Data Availability Statement

All data presented in this manuscript and the Supporting Information S1 are publicly available at <https://doi.org/10.4211/hs.b143432cfe72462fac90376631c9a2b3>.

Acknowledgments

The authors are grateful to Sarah Nelson, Susanne Schneider, Benoît Demars, and Jose-Luis Gerrero Calidonio for field work and practical assistance, and to two anonymous reviewers whose comments contributed to significantly improve this manuscript. The onsite logistical support by M. Sønsteby for regular grab sampling is gratefully acknowledged. This work has been supported by NIVA Strategiske instituttsatsinger fund, project #O-17012 Greensense.

References

- Ades, M., Adler, R., Allan, R., Allan, R. P., Anderson, J., Argüez, A., et al. (2020). Global climate. *Bulletin of the American Meteorological Society*, 101(8), S9–S128. <https://doi.org/10.1175/BAMS-D-20-0104.1>
- Arndt, S., Jørgensen, B. B., LaRowe, D. E., Middelburg, J. J., Pancost, R. D., & Regnier, P. (2013). Quantifying the degradation of organic matter in marine sediments: A review and synthesis. *Earth-Science Reviews*, 123, 53–86. <https://doi.org/10.1016/j.earscirev.2013.02.008>
- Bartosiewicz, M., Laurion, I., Clayer, F., & Maranger, R. (2016). Heat-Wave effects on oxygen, nutrients, and phytoplankton can alter global warming potential of gases emitted from a small shallow lake. *Environmental Science & Technology*, 50(12), 6267–6275. <https://doi.org/10.1021/acs.est.5b06312>
- Bastviken, D., Sundgren, I., Natchimuthu, S., Reyier, H., & Gålfalk, M. (2015). Cost-efficient approaches to measure carbon dioxide (CO₂) fluxes and concentrations in terrestrial and aquatic environments using mini loggers. *Biogeosciences*, 12, 3849–3859. <https://doi.org/10.5194/bg-12-3849-2015>
- Bogard, M. J., del Giorgio, P. A., Boutet, L., Chaves, M. C. G., Prairie, Y. T., Merante, A., & Derry, A. M. (2014). Oxidic water column methanogenesis as a major component of aquatic CH₄ fluxes. *Nature Communications*, 5(1), 5350. <https://doi.org/10.1038/ncomms6350>
- Braaten, H. F. V., Brecke Gundersen, C., Kaste, Ø., Sample, J., Øystein Hjermmann, D., Selvik, J. R., et al. (2020). *The Norwegian river monitoring programme 2019—Water quality status and trends*. Norsk institutt for vannforskning.
- Bruggeman, J., & Bolding, K. (2014). A general framework for aquatic biogeochemical models. *Environmental Modelling & Software*, 61, 249–265. <https://doi.org/10.1016/j.envsoft.2014.04.002>
- Butman, D., Stackpoole, S., Stets, E., McDonald, C. P., Clow, D. W., & Striegl, R. G. (2016). Aquatic carbon cycling in the conterminous United States and implications for terrestrial carbon accounting. *Proceedings of the National Academy of Sciences*, 113(1), 58–63. <https://doi.org/10.1073/pnas.1512651112>
- Butterbach-Bahl, K., Baggs, E. M., Dannenmann, M., Kiese, R., & Zechmeister-Boltenstern, S. (2013). Nitrous oxide emissions from soils: How well do we understand the processes and their controls? *Philosophical Transactions of the Royal Society B: Biological Sciences*, 368(1621), 20130122. <https://doi.org/10.1098/rstb.2013.0122>
- Campeau, A., Wallin, M. B., Giesler, R., Löfgren, S., Mörth, C.-M., Schiff, S., et al. (2017). Multiple sources and sinks of dissolved inorganic carbon across Swedish streams, refocusing the lens of stable C isotopes. *Scientific Reports*, 7(1), 9158. <https://doi.org/10.1038/s41598-017-09049-9>
- Catalán, N., Marcé, R., Kothawala, D. N., & Tranvik, L. J. (2016). Organic carbon decomposition rates controlled by water retention time across inland waters. *Nature Geoscience*, 9(7), 501–504. <https://doi.org/10.1038/ngeo2720>
- Chi, J., Nilsson, M. B., Laudon, H., Lindroth, A., Wallerman, J., Fransson, J. E. S., et al. (2020). The net landscape carbon balance—Integrating terrestrial and aquatic carbon fluxes in a managed boreal forest landscape in Sweden. *Global Change Biology*, 26(4), 2353–2367. <https://doi.org/10.1111/gcb.14983>
- Chmiel, H. E., Kokic, J., Denfeld, B. A., Einarsdóttir, K., Wallin, M. B., Koehler, B., et al. (2016). The role of sediments in the carbon budget of a small boreal lake. *Limnology & Oceanography*, 61(5), 1814–1825. <https://doi.org/10.1002/lno.10336>
- Ciais, P., Sabine, C., Bala, G., Bopp, L., Brovkin, V., Canadell, J., et al. (2013). Carbon and other biogeochemical cycles. In T. F. Stocker, D. Qin, G.-K. Plattner, M. Tignor, S. K. Allen, J. Boschung, et al. (Eds.), *Climate change 2013: The physical science basis. Contribution of working group I to the fifth assessment report of the intergovernmental panel on climate change* (pp. 465–570). Cambridge University Press. <https://doi.org/10.1017/CBO9781107415324.015>
- Cole, J. J., & Caraco, N. F. (1998). Atmospheric exchange of carbon dioxide in a low-wind oligotrophic lake measured by the addition of SF₆. *Limnology & Oceanography*, 43(4), 647–656. <https://doi.org/10.4319/lno.1998.43.4.0647>
- Cole, J. J., Prairie, Y. T., Caraco, N. F., McDowell, W. H., Tranvik, L. J., Striegl, R. G., et al. (2007). Plumbing the global carbon cycle: Integrating inland waters into the terrestrial carbon budget. *Ecosystems*, 10(1), 172–185. <https://doi.org/10.1007/s10021-006-9013-8>
- Cory, R. M., Ward, C. P., Crump, B. C., & Kling, G. W. (2014). Sunlight controls water column processing of carbon in arctic fresh waters. *Science*, 345(6199), 925–928. <https://doi.org/10.1126/science.1253119>
- Couture, R.-M., de Wit, H. A., Tominaga, K., Kiuru, P., & Markelov, I. (2015). Oxygen dynamics in a boreal lake responds to long-term changes in climate, ice phenology, and DOC inputs: Oxygen dynamics in a boreal lake. *Journal of Geophysical Research: Biogeosciences*, 120(11), 2441–2456. <https://doi.org/10.1002/2015JG003065>
- Crusius, J., & Wanninkhof, R. (2003). Gas transfer velocities measured at low wind speed over a lake. *Limnology & Oceanography*, 48(3), 1010–1017. <https://doi.org/10.4319/lno.2003.48.3.1010>
- de Wit, H. A., Austnes, K., Høyen, G., & Dalsgaard, L. (2015). A carbon balance of Norway: Terrestrial and aquatic carbon fluxes. *Biogeochemistry*, 123(1–2), 147–173. <https://doi.org/10.1007/s10533-014-0060-5>
- de Wit, H. A., Couture, R.-M., Jackson-Blake, L., Futter, M. N., Valinia, S., Austnes, K., et al. (2018). Pipes or chimneys? For carbon cycling in small boreal lakes, precipitation matters most. *Limnology and Oceanography Letters*, 3(3), 275–284. <https://doi.org/10.1002/lol2.10077>
- de Wit, H. A., Granhus, A., Lindholm, M., Kainz, M. J., Lin, Y., Braaten, H. F. V., & Blaszczyk, J. (2014). Forest harvest effects on mercury in streams and biota in Norwegian boreal catchments. *Forest Ecology and Management*, 324, 52–63. <https://doi.org/10.1016/j.foreco.2014.03.044>
- de Wit, H. A., Ledesma, J. L. J., & Futter, M. N. (2016). Aquatic DOC export from subarctic Atlantic blanket bog in Norway is controlled by sea salt deposition, temperature and precipitation. *Biogeochemistry*, 127(2), 305–321. <https://doi.org/10.1007/s10533-016-0182-z>
- de Wit, H. A., Valinia, S., Weyhenmeyer, G. A., Futter, M. N., Kortelainen, P., Austnes, K., et al. (2016). Current browning of surface waters will be further promoted by wetter climate. *Environmental Science and Technology Letters*, 3(12), 430–435. <https://doi.org/10.1021/acs.estlett.6b00396>
- DelSontro, T., Beaulieu, J. J., & Downing, J. A. (2018). Greenhouse gas emissions from lakes and impoundments: Upscaling in the face of global change: GHG emissions from lakes and impoundments. *Limnology and Oceanography Letters*, 3(3), 64–75. <https://doi.org/10.1002/lol2.10073>
- DelSontro, T., Boutet, L., St-Pierre, A., del Giorgio, P. A., & Prairie, Y. T. (2016). Methane ebullition and diffusion from northern ponds and lakes regulated by the interaction between temperature and system productivity: Productivity regulates methane lake flux. *Limnology & Oceanography*, 61(S1), S62–S77. <https://doi.org/10.1002/lno.10335>
- Deluca, T. H., & Boisvenue, C. (2012). Boreal forest soil carbon: Distribution, function and modelling. *Forestry*, 85(2), 161–184. <https://doi.org/10.1093/forestry/cps003>
- Denfeld, B. A., Klaus, M., Laudon, H., Sponseller, R. A., & Karlsson, J. (2018). Carbon dioxide and methane dynamics in a small boreal lake during winter and spring melt events. *Journal of Geophysical Research: Biogeosciences*, 123(8), 2527–2540. <https://doi.org/10.1029/2018JG004622>
- Denfeld, B. A., Wallin, M. B., Sahlée, E., Sobek, S., Kokic, J., Chmiel, H. E., & Weyhenmeyer, G. A. (2015). Temporal and spatial carbon dioxide concentration patterns in a small boreal lake in relation to ice-cover dynamics. *Boreal Environment Research*, 20(6), 679–692.

- Einarsdottir, K., Wallin, M. B., & Sobek, S. (2017). High terrestrial carbon load via groundwater to a boreal lake dominated by surface water inflow. *Journal of Geophysical Research: Biogeosciences*, 122(1), 15–29. <https://doi.org/10.1002/2016JG003495>
- Feng, M., Pusch, M., & Venohr, M. (2018). Estimating water residence time distribution in river networks by boosted regression trees (BRT) model. *Hydrology and Earth System Sciences Discussions*, 1–27. <https://doi.org/10.5194/hess-2018-309>
- Fernandes Sanches, L., Guenet, B., Marinho, C. C., Barros, N., & de Assis Esteves, F. (2019). Global regulation of methane emission from natural lakes. *Scientific Reports*, 9(1), 255. <https://doi.org/10.1038/s41598-018-36519-5>
- Guérin, F., Abril, G., Serça, D., Delon, C., Richard, S., Delmas, R., et al. (2007). Gas transfer velocities of CO₂ and CH₄ in a tropical reservoir and its river downstream. *Journal of Marine Systems*, 66(1), 161–172. <https://doi.org/10.1016/j.jmarsys.2006.03.019>
- Hastie, A., Lauerwald, R., Weyhenmeyer, G., Sobek, S., Verpoorter, C., & Regnier, P. (2018). CO₂ evasion from boreal lakes: Revised estimate, drivers of spatial variability, and future projections. *Global Change Biology*, 24(2), 711–728. <https://doi.org/10.1111/gcb.13902>
- Heiskanen, J. J., Mammarella, I., Haapanala, S., Pumpanen, J., Vesala, T., MacIntyre, S., & Ojala, A. (2014). Effects of cooling and internal wave motions on gas transfer coefficients in a boreal lake. *Tellus B: Chemical and Physical Meteorology*, 66(1), 22827. <https://doi.org/10.3402/tellusb.v66.22827>
- Hilton, R. G., Galy, A., Hovius, N., Horng, M.-J., & Chen, H. (2011). Efficient transport of fossil organic carbon to the ocean by steep mountain rivers: An orogenic carbon sequestration mechanism. *Geology*, 39(1), 71–74. <https://doi.org/10.1130/G31352.1>
- Holgerson, M. A., & Raymond, P. A. (2016). Large contribution to inland water CO₂ and CH₄ emissions from very small ponds. *Nature Geoscience*, 9(3), 222–226. <https://doi.org/10.1038/ngeo2654>
- Horgby, Å., Segatto, P. L., Bertuzzo, E., Lauerwald, R., Lehner, B., Ulseth, A. J., et al. (2019). Unexpected large evasion fluxes of carbon dioxide from turbulent streams draining the world's mountains. *Nature Communications*, 10(1), 4888. <https://doi.org/10.1038/s41467-019-12905-z>
- Hotchkiss, E. R., Hall, R. O., Jr., Sponseller, R. A., Butman, D., Klaminder, J., Laudon, H., et al. (2015). Sources of and processes controlling CO₂ emissions change with the size of streams and rivers. *Nature Geoscience*, 8(9), 696–699. <https://doi.org/10.1038/ngeo2507>
- Huguet, C., Smittenberg, R. H., Boer, W., Damsté, S., & Schouten, S. (2007). Twentieth century proxy records of temperature and soil organic matter input in the Drammensfjord, southern Norway. *Organic Geochemistry*, 38(11), 1838–1849. <https://doi.org/10.1016/j.orggeochem.2007.06.015>
- Karlsson, J., Giesler, R., Persson, J., & Lundin, E. (2013). High emission of carbon dioxide and methane during ice thaw in high latitude lakes. *Geophysical Research Letters*, 40(6), 1123–1127. <https://doi.org/10.1002/grl.50152>
- Kaste, Ø., Austnes, K., & de Wit, H. A. (2020). Streamwater responses to reduced nitrogen deposition at four small upland catchments in Norway. *Ambio*, 49(11), 1759–1770. <https://doi.org/10.1007/s13280-020-01347-3>
- Kortelainen, P., Larmola, T., Rantakari, M., Juutinen, S., Alm, J., & Martikainen, P. J. (2020). Lakes as nitrous oxide sources in the boreal landscape. *Global Change Biology*, 26(3), 1432–1445. <https://doi.org/10.1111/gcb.14928>
- Kraemer, B. M., Chandra, S., Dell, A. I., Dix, M., Kuusisto, E., Livingstone, D. M., et al. (2017). Global patterns in lake ecosystem responses to warming based on the temperature dependence of metabolism. *Global Change Biology*, 23(5), 1881–1890. <https://doi.org/10.1111/gcb.13459>
- Lawrence, D. M., Fischer, R., Koven, C. D., & Oleson, K. (2018). *Technical Description of version 5.0 of the Community Land Model (CLM)*. NCAR Technical Note.
- MacIntyre, S., Jonsson, A., Jansson, M., Aberg, J., Turney, D. E., & Miller, S. D. (2010). Buoyancy flux, turbulence, and the gas transfer coefficient in a stratified lake. *Geophysical Research Letters*, 37. (24). <https://doi.org/10.1029/2010GL044164>
- MacIntyre, S., Wanninkhof, R., & Chanton, J. P. (1995). Trace gas exchange across the air-water interface in freshwater and coastal marine environments. In *Biogenic Trace gases: Measuring emissions from soil and water* (pp. 52–97). John Wiley & Sons.
- Mattsson, T., Kortelainen, P., & Råike, A. (2005). Export of DOM from boreal catchments: Impacts of land use cover and climate. *Biogeochemistry*, 76(2), 373–394. <https://doi.org/10.1007/s10533-005-6897-x>
- Natchimuthu, S., Sundgren, I., Gålfalk, M., Klemmedtsson, L., & Bastviken, D. (2017). Spatiotemporal variability of lake pCO₂ and CO₂ fluxes in a hemiboreal catchment. *Journal of Geophysical Research: Biogeosciences*, 122(1), 30–49. <https://doi.org/10.1002/2016JG003449>
- Natchimuthu, S., Wallin, M. B., Klemmedtsson, L., & Bastviken, D. (2017). Spatio-temporal patterns of stream methane and carbon dioxide emissions in a hemiboreal catchment in Southwest Sweden. *Scientific Reports*, 7. <https://doi.org/10.1038/srep39729>
- Nelder, J. A., & Mead, R. (1965). A simplex method for function minimization. *The Computer Journal*, 7(4), 308–313. <https://doi.org/10.1093/comjnl/7.4.308>
- Neumann, T., & Schernewski, G. (2008). Eutrophication in the Baltic Sea and shifts in nitrogen fixation analyzed with a 3D ecosystem model. *Journal of Marine Systems*, 74(1), 592–602. <https://doi.org/10.1016/j.jmarsys.2008.05.003>
- Neumann, T., Wolfgang, F., & Christine, K. (2002). Experimental simulations with an ecosystem model of the Baltic Sea: A nutrient load reduction experiment. *Global Biogeochemical Cycles*, 16, 7. <https://doi.org/10.1029/2001GB001450>
- Öquist, M. G., Bishop, K., Grelle, A., Klemmedtsson, L., Köhler, S. J., Laudon, H., et al. (2014). The full annual carbon balance of boreal forests is highly sensitive to precipitation. *Environmental Science and Technology Letters*, 1(7), 315–319. <https://doi.org/10.1021/ez500169j>
- Randerson, J. T., Collatz, G. J., Fessenden, J. E., Munoz, A. D., Still, C. J., Berry, J. A., et al. (2002). A possible global covariance between terrestrial gross primary production and ¹³C discrimination: Consequences for the atmospheric ¹³C budget and its response to ENSO: ¹³C discrimination and ENSO. *Global Biogeochemical Cycles*, 16(4), 83–1–83–16. <https://doi.org/10.1029/2001GB001845>
- Randerson, J. T., Hoffman, F. M., Thornton, P. E., Mahowald, N. M., Lindsay, K., Lee, Y.-H., et al. (2009). Systematic assessment of terrestrial biogeochemistry in coupled climate-carbon models. *Global Change Biology*, 15(10), 2462–2484. <https://doi.org/10.1111/j.1365-2486.2009.01912.x>
- Rasilo, T., Prairie, Y. T., & Giordani, P. A. (2015). Large-scale patterns in summer diffusive CH₄ fluxes across boreal lakes, and contribution to diffusive C emissions. *Global Change Biology*, 21(3), 1124–1139. <https://doi.org/10.1111/gcb.12741>
- Robertson, D. M., agotzkie, R. A., & Magnuson, J. J. (1992). Lake ice records used to detect historical and future climatic changes. *Climatic Change*, 21, 407–427. <https://doi.org/10.1007/BF00141379>
- Robertson, D. M., & Ragotzkie, R. A. (1990). Changes in the thermal structure of moderate to large sized lakes in response to changes in air temperature. *Aquatic Sciences*, 52(4), 360–380. <https://doi.org/10.1007/BF00879763>
- Rucinski, D., Depinto, J. V., Scavia, D., & Beletsky, D. (2014). Modeling Lake Erie's hypoxia response to nutrient loads and physical variability. *Journal of Great Lakes Research*, 40, 151–161. <https://doi.org/10.1016/j.jglr.2014.02.003>
- Schelker, J., Singer, G. A., Ulseth, A. J., Hengsberger, S., & Battin, T. J. (2016). CO₂ evasion from a steep, high gradient stream network: Importance of seasonal and diurnal variation in aquatic pCO₂ and gas transfer. *Limnology & Oceanography*, 61(5), 1826–1838. <https://doi.org/10.1002/lno.10339>
- SFT. (2009). *The Norwegian monitoring programme for long-range transported air pollutants*. The Norwegian Pollution Control Authority (SFT).
- Smith, R. W., Bianchi, T. S., Allison, M., Savage, C., & Galy, V. (2015). High rates of organic carbon burial in fjord sediments globally. *Nature Geoscience*, 8(6), 450–453. <https://doi.org/10.1038/ngeo2421>

- Smittenberg, R. H., Baas, M., Green, M. J., Hopmans, E. C., Schouten, S., & Sinninghe Damsté, J. S. (2005). Pre- and post-industrial environmental changes as revealed by the biogeochemical sedimentary record of Drammensfjord, Norway. *Marine Geology*, 214(1), 177–200. <https://doi.org/10.1016/j.margeo.2004.10.029>
- Solheim, A. L., Schartau, A. K., Bongard, T., Bækkeli, K. A. E., Dahl-Hansen, G., Demars, B. O. L., et al. (2019). *Økoston 2018: Basisovervåking av store innsjøer. Utprøving av metodikk for overvåking og klassifisering av økologisk tilstand i henhold til vannforskriften*. Retrieved from <https://niva.brage.unit.no/niva-xmlui/handle/11250/2642181>
- Solheim, A. L., Schartau, A. K., Bongard, T., Bækkeli, K. A. E., Dahl-Hansen, G., Demars, B. O. L., et al. (2020). *ØKOSTOR 2019: Basisovervåking av store innsjøer. Utprøving av metodikk for overvåking og klassifisering av økologisk tilstand i henhold til vannforskriften*. Norsk institutt for vannforskning. Retrieved from <https://niva.brage.unit.no/niva-xmlui/handle/11250/2720472>
- Stahr, P. A., Testa, J. M., Kemp, W. M., Cole, J. J., Sand-Jensen, K., & Smith, S. V. (2012). The metabolism of aquatic ecosystems: History, applications, and future challenges. *Aquatic Sciences*, 74(1), 15–29. <https://doi.org/10.1007/s00027-011-0199-2>
- Stumm, W., & Morgan, J. J. (1996). *Aquatic chemistry: Chemical equilibria and rates in natural waters* (3rd ed.). Wiley.
- Tissot, B. P., & Welte, D. H. (1984). *Petroleum formation and occurrence* (2nd ed.). Springer-Verlag. <https://doi.org/10.1007/978-3-642-87813-8>
- Ulseth, A., Hall, R., Canadell, M. B., Madinger, H., Niayifar, A., & Battin, T. (2019). Distinct air–water gas exchange regimes in low- and high-energy streams. *Nature Geoscience*, 12(4), 259–263.
- Vachon, D., & Prairie, Y. T. (2013). The ecosystem size and shape dependence of gas transfer velocity versus wind speed relationships in lakes. *Canadian Journal of Fisheries and Aquatic Sciences*, 70(12), 1757–1764. <https://doi.org/10.1139/cjfas-2013-0241>
- Verpoorter, C., Kutser, T., Seekell, D. A., & Tranvik, L. J. (2014). A global inventory of lakes based on high-resolution satellite imagery. *Geophysical Research Letters*, 41(18), 6396–6402. <https://doi.org/10.1002/2014GL060641>
- Wallin, M. B., Campeau, A., Audet, J., Bastviken, D., Bishop, K., Kocik, J., et al. (2018). Carbon dioxide and methane emissions of Swedish low-order streams—A national estimate and lessons learnt from more than a decade of observations. *Limnology and Oceanography Letters*, 3(3), 156–167. <https://doi.org/10.1002/lol2.10061>
- Wanninkhof, R. (2014). Relationship between wind speed and gas exchange over the ocean revisited. *Limnology and Oceanography: Methods*, 12(6), 351–362. <https://doi.org/10.4319/lom.2014.12.351>
- Ward, N. D., Bianchi, T. S., Medeiros, P. M., Seidel, M., Richey, J. E., Keil, R. G., & Sawakuchi, H. O. (2017). Where carbon goes when water flows: Carbon cycling across the aquatic continuum. *Frontiers in Marine Science*, 4. <https://doi.org/10.3389/fmars.2017.00007>
- Webb, J. R., Santos, I. R., Maher, D. T., & Finlay, K. (2019). The importance of aquatic carbon fluxes in net ecosystem carbon budgets: A catchment-scale review. *Ecosystems*, 22(3), 508–527. <https://doi.org/10.1007/s10021-018-0284-7>
- Weyhenmeyer, G. A., Fröberg, M., Karlun, E., Khalili, M., Kothawala, D., Temnerud, J., & Tranvik, L. J. (2012). Selective decay of terrestrial organic carbon during transport from land to sea. *Global Change Biology*, 18(1), 349–355. <https://doi.org/10.1111/j.1365-2486.2011.02544.x>
- Weyhenmeyer, G. A., Kortelainen, P., Sobek, S., Müller, R., & Rantakari, M. (2012). Carbon dioxide in boreal surface waters: A comparison of lakes and streams. *Ecosystems*, 15(8), 1295–1307. <https://doi.org/10.1007/s10021-012-9585-4>
- Wik, M., Varner, R. K., Anthony, K. W., MacIntyre, S., & Bastviken, D. (2016). Climate-sensitive northern lakes and ponds are critical components of methane release. *Nature Geoscience*, 9, 99–105. <https://doi.org/10.1038/ngeo2578>
- Wilhelm, E., Battino, R., & Wilcock, R. J. (1977). Low-pressure solubility of gases in liquid water. *Chemical Reviews*, 77(2), 219–262. <https://doi.org/10.1021/cr60306a003>
- Winslow, L. A., Zwart, J. A., Batt, R. D., Dugan, H. A., Woolway, R. I., Corman, J. R., et al. (2016). Lake metabolizer: An R package for estimating lake metabolism from free-water oxygen using diverse statistical models. *Inland Waters*, 6(4), 622–636. <https://doi.org/10.1080/IW-6.4.883>
- Yang, H., Andersen, T., Dörsch, P., Tominaga, K., Thrane, J.-E., & Hessen, D. O. (2015). Greenhouse gas metabolism in Nordic boreal lakes. *Biogeochemistry*, 126(1–2), 211–225. <https://doi.org/10.1007/s10533-015-0154-8>

Reference From the Supporting Information

- Engeland, K., Engen-Skaugen, T., Haugen, J., Beldring, S., & Førland, E. (2004). *Comparison of evaporation estimated by the HIRHAM and GWB models for present climate and climate change scenarios (No. 17/2004)*. Norwegian Meteorological Institute. Retrieved from https://www.met.no/publikasjoner/met-report/met-report-2004/_attachment/download/b3ea4682-9ce8-4082-9ad1-ed9dacf28b69:fc812847ce8e8f-f8407d3f1e9a8b015c76ad8146/MET-report-17-2004.pdf